

PAPER

# Dynamics and performance of a two degree-of-freedom galloping-based piezoelectric energy harvester

To cite this article: Chunbo Lan *et al* 2019 *Smart Mater. Struct.* **28** 045018

View the [article online](#) for updates and enhancements.

## You may also like

- [Enhancing galloping-based energy harvesting through expanded quasi-zero-stiffness region](#)  
Chunbo Lan, Ye Zhang, Shuo Wang *et al.*
- [Energy harvesting from transverse galloping using a two-degree-of-freedom flow energy harvester](#)  
Igoke Major, P J Tan and Ali Abolfathi
- [Modeling and experimental investigation of asymmetric distance with magnetic coupling based on galloping piezoelectric energy harvester](#)  
Huirong Zhang, Leian Zhang, Yuanbo Wang *et al.*

# Dynamics and performance of a two degree-of-freedom galloping-based piezoelectric energy harvester

Chunbo Lan<sup>1</sup> , Lihua Tang<sup>2</sup> , Guobiao Hu<sup>2</sup> and Weiyang Qin<sup>3</sup>

<sup>1</sup> College of Aerospace Engineering, Nanjing University of Aeronautics and Astronautics, Nanjing, People's Republic of China

<sup>2</sup> Department of Mechanical Engineering, The University of Auckland, New Zealand

<sup>3</sup> Department of Engineering Mechanics, Northwestern Polytechnical University, Xi'an, People's Republic of China

E-mail: [chunbolan@nuaa.edu.cn](mailto:chunbolan@nuaa.edu.cn)

Received 14 September 2018, revised 18 January 2019

Accepted for publication 19 February 2019

Published 20 March 2019



CrossMark

## Abstract

To improve the performance of the galloping based piezoelectric energy harvester (GEPH), this paper analytically investigates the potential advantages of the 2-degree-of-freedom (2-DOF) GPEHs over the conventional 1-DOF GPEH. Firstly, two different configurations of 2-DOF GPEH are proposed and the corresponding governing equations are presented. The approximate analytical solutions to both configurations are derived by using the harmonic balance method. Numerical simulations are conducted to verify the accuracy of these analytical solutions. Subsequently, comparisons are conducted between the 1-DOF GPEH and the 2-DOF GPEHs in terms of the cut-in wind speeds and output powers. It is demonstrated, both analytically and numerically, that the second configuration of 2-DOF GPEH can easily and remarkably reduce the cut-in wind speed and improve the output power from galloping phenomenon. Finally, a parametric study is performed to ascertain the effects of the mechanical parameters of the second configuration on the energy harvesting performance. Based on the results from the parametric study, design guidelines for tuning the mechanical parameters are provided to achieve performance enhancement.

Keywords: wind energy harvesting, piezoelectric, galloping

(Some figures may appear in colour only in the online journal)

## 1. Introduction

In the past few decades, the demands of micro-electronics, such as wireless sensor and portable electronics are rapidly increased. To provide a sustainable and reliable power for these small devices, researchers have been attracted to design energy harvesters [1–9] for capturing the renewable energy from the environment. Aeroelastic energy harvesting [1, 7] is one of the most promising technologies for micro-scale power devices in recent years, since the efficiency of traditional rotary type wind turbines drops significantly with the decrease of the size [7].

For the aeroelastic energy harvesters, the wind energy needs to be converted into the form of aeroelastic vibrations. Piezoelectric or electromagnetic transducers can then convert

vibrations and generate electricity. A variety of mechanisms for converting the wind energy into vibrations, including vortex-induced vibration [1, 6, 10], flutter [11, 12], galloping [13–18] and wake galloping [19–21], have been employed to improve the efficiency of energy harvesting. Among these mechanisms, the galloping phenomenon is the most widely utilised and investigated due to the large oscillation amplitudes and high efficiency [18]. There are normally two main objectives in the design of the galloping energy harvesters: one is to decrease the cut-in wind speed so that the low-speed wind energy widely existing in our environment can be harnessed; the other is to improve the output power. Conventional single degree-of-freedom (DOF) galloping energy harvester, which consists of an elastic bluff body and a

piezoelectric/electromagnetic transducer, has been well studied in the past few years. The feasibility of galloping energy harvesting was theoretically demonstrated by Barrero-Gil *et al* [13], which was experimentally validated by Sirohi *et al* [22]. In Sirohi's research, a beam with a D-shaped cross-section bluff body and piezoelectric patches embedded was utilised to harvest the wind energy based on the galloping phenomenon. In that research, it was shown that the power output increased rapidly with the increase of the wind speed when galloping occurred. To further improve the efficiency, the geometry of bluff body was designed as triangle section [23], square section [24] etc. The influence of the cross-section geometry on the performance of a galloping piezoelectric energy harvester was experimentally investigated by Yang *et al* [16]. It was revealed that the performance of square cross section geometry is better than that of the triangles, D-section and rectangle geometries.

To investigate the dynamic characteristics and performance of GPEH, various methods have been used in the modelling and analysis of GPEH. Zhao *et al* [25] conducted a comparative study on different modelling methods (including lumped-parameter model and distributed parameter model) of the galloping piezoelectric energy harvester. It was found that the lumped-parameter model was preferable due to the simplicity and the convenience to identify the parameters from experiments. Abdelkefi *et al* [26] utilised the normal form to characterise the Hopf bifurcation of GPEH and it was noted that the maximum power harvested from galloping was always accompanied by minimum displacements of bluff body. To accurately represent the aerodynamic force of galloping, Parkinson *et al* [27] established a nonlinear aerodynamic force model based on the quasi-steady hypothesis. Later, Barrero *et al* [13] simplified this model by using a cubic polynomial expression in the theoretical analysis. Javed *et al* [28] compared the influences of different aerodynamic force models on the performance of GPEH. It was found that the aerodynamic forces determined by the same experimental data based on different models can result in variations in the dynamic response of GPEH. To ascertain the effect of the load resistance on the cut-in wind speed and output power of GPEH, Zhao *et al* [29] introduced the equivalent circuit representation approach to analyse the interactions between the mechanical and electrical domains of GPEH. The relations between the resistance of the AC/DC interface circuit and the cut-in wind speed, the output power were revealed. Abdelkefi *et al* [14] proposed a nonlinear distributed-parameter model to determine the effect of the load resistance on the harvested power. Tan and Yan [30] derived the analytical solutions to Abdelkefi's model by using the harmonic balance method and optimised the performance of the GPEH in terms of the output power. Bibo and Daqaq [18] derived the approximate analytical solution to the lumped-parameter model of 1-DOF GPEH by using the multi-scale method and established an analytical framework to identify the influence of important parameters on the dynamic responses and performance. Zhao and Yang [31] derived the analytical solutions to a GPEH

interfaced with three different circuits, including AC, Standard and SCE circuits. The applicabilities of different circuits for power optimisation were discussed. Moreover, the responses of the 1-DOF GPEH subjected to both the base excitation and wind have been experimentally [32] and analytically [18, 33, 34] investigated. It was observed that the quenching phenomenon due to the increase of the base excitation could suppress the galloping, resulting in a decrease of the output power.

To further increase the efficiency of aeroelastic energy harvesting, structural nonlinearity started to gain attentions recently due to the great success of its application in vibration energy harvesting [5, 8, 35, 36]. A nonlinear restoring force was introduced into galloping energy harvesting by Bibo *et al* [17]. It was revealed that the inter-well oscillation of the bistable configuration clearly outperformed the high-energy oscillation of the monostable configuration. Such a nonlinear restoring force was also utilised in the wake galloping energy harvesting by Alhadidi *et al* [21]. Results indicated that the proposed nonlinear energy harvester can largely broaden the bandwidth. Naseer *et al* [37] proposed a monostable system to harvest the vortex-induced vibrations. It was shown that changing the nonlinear restoring force caused a shift of lock-in region, which was helpful for low speed wind energy harvesting. Meanwhile, impact was also introduced by Ewere *et al* [15] in the galloping energy harvesting to improve the service life of GPEH. However, the voltage reduction was inevitable. Zhao *et al* [38] recently proposed an impact-based energy harvester, which integrated the conventional GPEH with an elastic stopper to achieve broadband energy harvesting.

For the classic 1-DOF GPEH, since the circuit-induced damping is dependent on the frequency, the introduction of nonlinear stiffness or variation in stiffness will change the frequency and thus change the circuit induced damping. Hence, the change of stiffness or introducing nonlinear stiffness can influence the cut-in wind speed and it is intrinsically dependent on the electromechanical coupling. However, when the piezoelectric energy harvester is connected with a load resistance, the circuit-induced damping is non-negative [39], hence the cut-in wind speed of 1-DOF GPEH can never be reduced by changing stiffness or electromechanical coupling. The possible alternative means to decrease the cut-in wind speed of 1-DOF GPEH is to directly reduce the mechanical damping, which is usually beyond the control for a given transduction mechanism. Therefore, decreasing the cut-in wind speed is difficult, though it has been acknowledged that it is of great importance for low speed wind energy harvesting.

Meanwhile, Zhao *et al* [40], proposed a nonlinear 2-DOF GPEH which consists of an elastic bluff body, a cut-out cantilever and two magnets at the free end of the two cantilevers. It was revealed in the experiment that the cut-in wind speed was largely decreased and the harvested power was improved at the same time. However, due to the complexity of the structure design and the implementation of the nonlinear magnetic interactions, the analytical solution to this

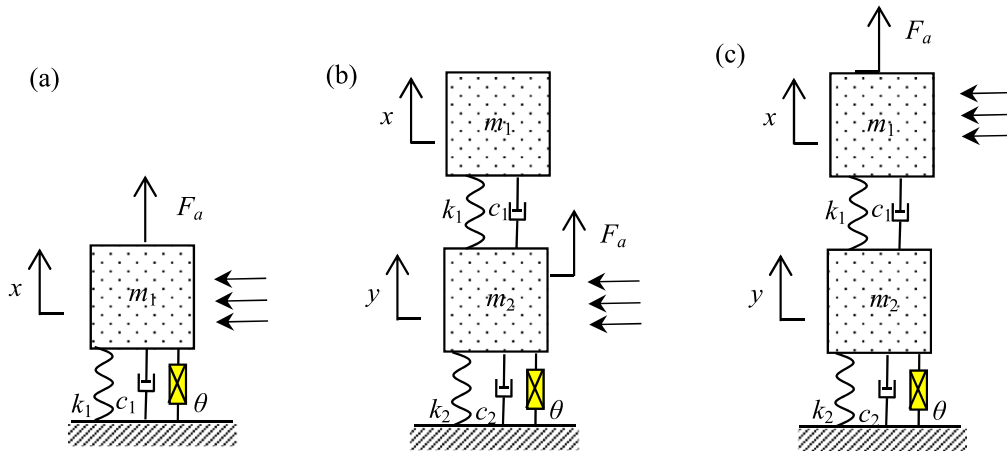


**Figure 1.** (a) Conventional 1-DOF GPEH; (b) the first configuration of 2-DOF GPEH; (c) the second configuration of 2-DOF GPEH.

nonlinear 2-DOF GPEH was not presented. The dynamic properties and energy harvesting performance of the 2-DOF GPEH, in addition of the effect of the nonlinear magnetic force are still open questions. To this end, this paper focuses on unlocking the dynamic properties and the energy harvesting performance of a 2-DOF oscillator with a piezoelectric transducer subjected to the galloping excitation. The content of this paper is organised as follows. Two configurations of 2-DOF GPEHs are proposed and the corresponding lumped parameter models are established in section 2. The approximate analytical solutions derived by using harmonic balance method are presented in section 3. A comparison study between the conventional 1-DOF GPEH and proposed 2-DOF GPEHs in terms of the energy harvesting performance is presented in section 4. A parametric analysis of the second configuration of 2-DOF GPEH is conducted in section 5. Some useful conclusions are drawn in section 6.

## 2. Galloping piezoelectric energy harvesters

Figure 1 shows the lumped parameter models of the conventional 1-DOF and our proposed 2-DOF GPEHs. The 1-DOF GPEH consists of an elastically mounted bluff body and a piezoelectric patch (figure 1(a)), which has been widely studied by many previous researches. It undergoes galloping in the transverse direction when subjected to an incoming uniform cross-flow. In this paper, a 2-DOF GPEH is developed based on the conventional 1-DOF GPEH. The first way is to add another 1-DOF oscillator on the top of conventional 1-DOF GPEH, as shown in figure 1(b). The second way is to replace the rigid support of 1-DOF GPEH with an elastic oscillator, as shown in figure 1(c). For the first configuration, the bottom mass is considered as the bluff body. While in the second configuration, the top mass is set to be the bluff body. As a result, the aerodynamic force is applied on mass  $m_2$  in configuration 1 and on mass  $m_1$  in configuration 2. In the practical design, for the first configuration, the additional oscillator can be implemented inside the bluff body so that the additional

oscillator will not interact with the wind flow. For the second configuration, the additional oscillator can be designed as a fixed-fixed beam with the additional mass in the middle made of metal so that its size is small and the interaction between this mass and wind flow can be minimised.  $F_a$  stands for the aerodynamic force induced by the external uniform cross-flow and depends on the geometry of bluff body. For convenience, the first configuration of 2-DOF GPEH shown in figure 1(b) is named as 2-DOF GPEH-1 while the second configuration of 2-DOF GPEH in figure 1(c) as 2-DOF GPEH-2. The comparison of the performances of 1-DOF and 2-DOF GPEHs are conducted in the following sections.

### 2.1. Conventional 1-DOF GPEH

The conventional 1-DOF GPEH has been deeply investigated in the past few years. For the modelling of the 1-DOF GPEH, based on the assumption of linear electromechanical coupling and elasticity behaviours, the governing equations of the lumped parameter model widely used in the literatures [16–18, 41] are:

$$\begin{cases} m_1 \ddot{x} + c_1 \dot{x} + k_1 x - \theta V = F_a \\ C_p \dot{V} + \frac{V}{R} + \theta \dot{x} = 0 \end{cases}, \quad (1)$$

where,  $m_1$ ,  $c_1$ , and  $k_1$ , are the effective mass, damping and stiffness of the 1-DOF GPEH, respectively. The effective damping can be expressed as  $c_1 = 2\zeta_1\omega_1 m_1$ , where  $\zeta_1$  is the damping ratio and  $\omega_1$  is the natural frequency;  $\theta$  is the electromechanical coupling coefficient;  $C_p$  is the clamped capacitance of the piezoelectric transducer;  $x$  is the displacement relative to the base;  $V$  is the voltage across the piezoelectric transducer;  $R$  is the resistance;  $F_a$  is the vertical component of the aerodynamic force acting on the bluff body.

To represent the aerodynamic force, the quasi-steady assumption is widely used in galloping energy harvesting. In the quasi-steady assumption [42], the motion of the bluff body is assumed to be very slow as compared to the motion of wind. Under this assumption, the coefficients of

aerodynamic force stay constant for a given angle of attack. According to Barrero-Gil [13], the aerodynamic force  $F_a$  can be modelled as

$$F_a = \frac{1}{2}\rho U^2 L D \left[ s_1 \frac{\dot{x}}{U} - s_3 \left( \frac{\dot{x}}{U} \right)^3 \right], \quad (2)$$

where  $L$  and  $D$  are the cross-flow length and width of the bluff body,  $\rho$  and  $U$  are the air density and wind speed respectively,  $s_1$  and  $s_3$  are the empirical linear and cubic coefficients of the transverse galloping force, which are dependent on the cross-section geometry of the prismatic structure. For the square case, these coefficients are determined by Parkinson and Smith [43].

Submitting equation (2) into equation (1), the governing equation of 1-DOF GPEH is rewritten as

$$\begin{cases} m_1 \ddot{x} + c_1 \dot{x} + k_1 x - \theta V = \frac{1}{2} \rho U L D \left[ s_1 \dot{x} - \frac{s_3}{U^2} (\dot{x})^3 \right] \\ C_p \dot{V} + \frac{V}{R} + \theta \dot{x} = 0 \end{cases} \quad (3)$$

## 2.2. 2-DOF GPEHs

Based on the modelling of 1-DOF GPEH, the governing equations of 2-DOF GPEH-1 (refers to figure 1(b)) can be quickly obtained as

$$\begin{cases} m_1 \ddot{x} + c_1 (\dot{x} - \dot{y}) + k_1 (x - y) = 0 \\ m_2 \ddot{y} + c_2 \dot{y} + k_2 y - \theta V = \frac{1}{2} \rho U L D \left[ s_1 \dot{y} - \frac{s_3}{U^2} (\dot{y})^3 \right. \\ \left. + c_1 (\dot{x} - \dot{y}) + k_1 (x - y) \right] \\ C_p \dot{V} + \frac{V}{R} + \theta \dot{y} = 0 \end{cases}, \quad (4)$$

where  $m_2$ ,  $c_2$ , and  $k_2$ , are the effective mass, damping and stiffness of the auxiliary oscillator, respectively,  $y$  is the displacement of the auxiliary oscillator.

Similarly, the governing equations of 2-DOF GPEH-2 (refers to figure 1(c)) are

$$\begin{cases} m_1 \ddot{x} + c_1 (\dot{x} - \dot{y}) + k_1 (x - y) \\ = \frac{1}{2} \rho U L D \left[ s_1 \dot{x} - \frac{s_3}{U^2} (\dot{x})^3 \right] \\ m_2 \ddot{y} + c_2 \dot{y} + k_2 y - \theta V = c_1 (\dot{x} - \dot{y}) + k_1 (x - y) \\ C_p \dot{V} + \frac{V}{R} + \theta \dot{y} = 0 \end{cases} \quad (5)$$

## 3. Harmonic balance analysis

### 3.1. Analytical solutions of the conventional 1-DOF GPEH

The approximate solution of the conventional 1-DOF GPEH (figure 1(a)) was derived in [18] by using the multi-scale

method. In this paper, the solution is derived by using the harmonic balance method. The detailed derivation for the 1-DOF case can be found in appendix and the results are

$$\begin{cases} m_1 \omega^2 - k_1 - \frac{c_p (\theta R \omega)^2}{(C_p R \omega)^2 + 1} = 0 \\ c_1 + \frac{\theta^2 R}{(C_p R \omega)^2 + 1} - \frac{1}{2} \rho U L D \left( s_1 - \frac{3}{4} \frac{s_3}{U^2} \omega^2 r^2 \right) = 0 \end{cases}, \quad (6)$$

where  $r$  stands for the amplitude of displacement response of 1-DOF GPEH and  $\omega$  is the corresponding frequency.

Since the circuit-induced stiffness and damping for a piezoelectric energy harvester are

$$\begin{cases} k_e = \frac{C_p (\theta R \omega)^2}{(C_p R \omega)^2 + 1} \\ c_e = \frac{\theta^2 R}{(C_p R \omega)^2 + 1} \end{cases}. \quad (7)$$

Equation (6) can be simplified as

$$\begin{cases} m_1 \omega^2 - k_1 - k_e = 0 \\ c_1 + c_e - \frac{1}{2} \rho U L D \left( s_1 - \frac{3}{4} \frac{s_3}{U^2} \omega^2 r^2 \right) = 0 \end{cases}. \quad (8)$$

From the first expression of equation (8), it is learned that the frequency of response mainly depends on the mechanical stiffness and electric circuit-induced stiffness. Meanwhile, setting  $r = 0$  in the second expression of equation (8), the cut-in wind speed of 1-DOF GPEH is obtained as

$$U_{cr} = \frac{2(c_1 + c_e)}{\rho L D s_1}. \quad (9)$$

For a certain bluff body, its parameters, such as  $L$ ,  $D$ ,  $s_1$  and  $\rho$  are fixed. Hence, the cut-in wind speed simply depends on the mechanical damping and electrical damping. From equation (7), it can be seen that for any positive resistance, the electrical damping is non-negative. Therefore, the cut-in wind speed of the 1-DOF GPEH will never be smaller than that of the counterpart without piezoelectric components (the mechanical damping is assumed to be unchanged). As a result, there is no other way to reduce the cut-in wind speed for the conventional 1-DOF GPEH except for reducing the mechanical damping. This is one of the main facts that restrict the performance of the conventional 1-DOF GPEH for low-speed wind energy harvesting. To break through this limitation on the cut-in wind speed, 2-DOF GPEH is developed, whose cut-in wind speed is not only just dependant on the mechanical and electrical damping, but also closely related to other mechanical parameters, such as mass and stiffness. In practical applications, the adjustment can be easily achieved. In the following section, harmonic balance analysis is used to obtain the approximate analytical solutions of the two configurations of 2-DOF GPEHs and the comparison between the 1-DOF and 2-DOF GPEHs is also presented.

**Table 1.** Parameters of galloping piezoelectric energy harvester.

Mechanical parameters		Aerodynamic parameters	
Effective mass $m_1$ (g)	113.4	Air Density, $\rho$ (kg m <sup>-3</sup> )	1.24
Effective mass $m_2$ (g)	113.4	Bluff body height, $L$ (m)	0.1
Effective stiffness $k_1$ (N m <sup>-1</sup> )	58.02	Cross flow dimension, $D$ (m)	0.05
Effective stiffness $k_2$ (N m <sup>-1</sup> )	58.02	Linear aerodynamic coefficient, $s_1$	2.5
Damping ratio $\zeta_1$	0.003	Cubic aerodynamic coefficient, $s_3$	130
Damping ratio $\zeta_2$	0.003		
Electromechanical coupling $\theta$ ( $\mu\text{N V}^{-1}$ )	190		
Capacitance $C_p$ (nF)	187		

### 3.2. Analytical solutions of 2-DOF GPEH-1

To obtain the analytical solution of 2-DOF GPEH-1, the harmonic balance method is employed, and the details of derivation can be found in the [appendix](#). The approximate solutions are

$$\begin{cases} -m_2\omega^2 - c_1\omega q + \bar{k}_2 - k_1(p-1) = 0 \\ -\bar{c}_2\omega + c_1\omega(p-1) - k_1q + \frac{1}{2}\rho ULD \\ \left(s_1 - \frac{3}{4}\frac{s_3}{U^2}\omega^2 r_y^2\right)\omega = 0 \end{cases}, \quad (10)$$

where  $\bar{c}_2 = c_2 + c_e$ ,  $\bar{k}_2 = k_2 + k_e$ , coefficients  $p$  and  $q$  are defined by equation (A.17) in the [appendix](#). By solving equation (10), we can obtain the frequency of dynamic responses ( $\omega$ ) and the displacement amplitude  $r_y$  (defined by equation (A.18)). Setting the magnitude of displacement  $r_y = 0$ , the cut-in wind speed of the first configuration of 2-DOF GPEH is obtained from equation (10) and it is

$$U_{cr} = \left[ 2(c_2 + c_e) + \frac{2(m_1\omega^2)^2}{(k_1 - m_1\omega^2)^2 + (c_1\omega)^2} c_1 \right] / (\rho L D s_1). \quad (11)$$

To fairly compare the cut-in wind speed of 1-DOF GPEH and that of 2-DOF GPEH-1, the damping  $c_2$  of 2-DOF GPEH-1 is set to be the same with the damping  $c_1$  of 1-DOF GPEH since it is the primary DOF of 2-DOF GPEH-1 that converts the vibration energy into electricity. By comparing equation (9) and equation (11), it is revealed that the cut-in wind speed of 2-DOF GPEH-1 is always larger than that of conventional 1-DOF GPEH when the damping  $c_1$  of 2-DOF GPEH-1 is positive. As a result, in terms of cut-in wind speed, such a 2-DOF GPEH-1 is not favourable for low-speed wind energy harvesting.

### 3.3.3. Analytical solutions of 2-DOF GPEH-2

Similarly, the same procedure is employed to solve the approximate solutions of 2-DOF GPEH-2. The solutions are

$$\begin{cases} -m_1\omega^2 + c_1\omega\tilde{q} + k_1(1 - \tilde{p}) = 0 \\ k_1\tilde{q} - c_1\omega(1 - \tilde{p}) + \frac{1}{2}\rho ULD\omega \left(s_1 - \frac{3}{4}\frac{s_3}{U^2}\omega^2 r_x^2\right) = 0 \end{cases}, \quad (12)$$

where coefficients  $\tilde{p}$  and  $\tilde{q}$  are defined by equation (A.28) in the [appendix](#). From equation (12), we obtain the frequency of dynamic responses ( $\omega$ ) and the magnitudes of displacement responses  $r_x$  of 2-DOF GPEH-2 (defined by equation (A.29)). The cut-in wind speed of 2-DOF GPEH-2 is calculated from equation (12) by setting  $r_x = 0$ :

$$U_{cr} = \frac{-2k_1\tilde{q} + 2c_1\omega(1 - \tilde{p})}{\rho L D \omega s_1}. \quad (13)$$

To ensure that the cut-in wind speed of 2-DOF GPEH-2 is lower than that of conventional 1-DOF GPEH, the following condition should be satisfied:

$$-k_1\tilde{q} - c_1\omega\tilde{p} < 0. \quad (14)$$

From equation (13), it is learned that the cut-in wind speed depends on not only the mechanical damping of the original oscillator ( $c_1$ ), but also the damping ( $c_2$ ), stiffness ( $k_2$ ) and mass ( $m_2$ ) of the auxiliary oscillator. By properly adjusting the parameters of the auxiliary oscillator, the 2-DOF GPEH-2 is promising to have a much lower cut-in wind speed than the 1-DOF GPEH, which is helpful for low-speed wind energy harvesting.

## 4. Comparative study of 1-DOF GPEH and 2-DOF GPEHs

To show the potential advantages of 2-DOF GPEH, the conventional 1-DOF GPEH and that of the proposed 2-DOF GPEHs are analysed and compared in terms of the cut-in wind speed and generated power. The analytical solutions of the three configurations, along with numerical simulations, are calculated by using the experimental parameters in [17], which are listed in table 1. All the mechanical and electrical parameters of conventional 1-DOF GPEH and proposed 2-DOF GPEHs are set to be the same. For the 2-DOF GPEHs, the mass, damping ratio and stiffness of two sub-oscillators are set to be the same with that of 1-DOF GPEH, as listed in table 1. Moreover, since the 2-DOF GPEH has doubled the mass and components of the 1-DOF GPEH, for the fairness of comparison, another 1-DOF GPEH with its mass and bluff body doubled (named as 1-DOF GPEH-2) is also considered and compared with the 2-DOF GPEHs.

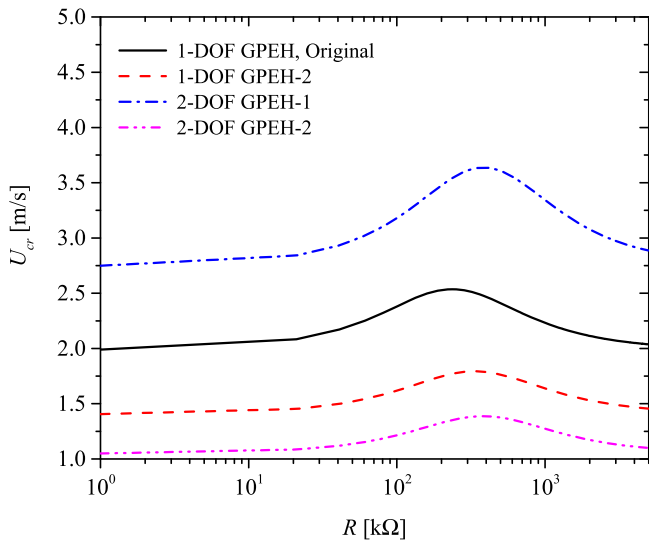


**Figure 2.** Cut-in wind speeds of four GPEH configurations for various resistances.

#### 4.1. Cut-in wind speed

Figure 2 compares the cut-in wind speeds of the four configurations with various resistances. For all the configurations, the cut-in wind speed in the short circuit condition is relatively low. As the resistance increases, the cut-in wind speed also increases until it reaches the peak value. Then, the further increase of the resistance decreases the cut-in wind speed. The potential reason of these characteristics is mainly due to the relation between the resistance and the circuit induced equivalent damping in equation (7). When it is close to the short circuit or open circuit, the equivalent damping is close to zero, which results in small cut-in wind speeds. In these cases, the piezoelectric component rarely provides circuit-induced damping. Thus, the cut-in wind speed of GPEH is close to that of the structure without piezoelectric component. Meanwhile, for a medium resistance, the circuit induced damping is not negligible, which is the main reason of the increase in the cut-in wind speeds. Generally speaking, the AC interface circuit (a pure resistor) has similar influences on both 1-DOF and 2-DOF GPEHs, which also indicates that the piezoelectric component with a pure resistance will increase the cut-in wind speed of both configurations.

From the comparison of the cut-in wind speeds of these systems as shown in figure 2, it is clearly seen that the 2-DOF GPEH-2 has the smallest  $U_{cr}$  and 2-DOF GPEH-1 has the largest  $U_{cr}$  among these four configurations. Though the cut-in wind speed of 1-DOF GPEH is largely decreased when the mass and size of bluff body are doubled, the proposed 2-DOF GPEH-2 has a better performance. For the short circuit condition, the cut-in wind speed of 2-DOF GPEH-2 is  $1.05 \text{ m s}^{-1}$ ,  $0.3575 \text{ m s}^{-1}$  less than that of the 1-DOF GPEH-2. When  $R = 161 \text{ k}\Omega$ , the  $U_{cr}$  of 2-DOF GPEH-2 is  $1.293 \text{ m s}^{-1}$ , which is  $0.473 \text{ m s}^{-1}$  less than that of 1-DOF GPEH-2 ( $1.766 \text{ m s}^{-1}$ ). While, the  $U_{cr}$  of 2-DOF GPEH-1 is  $3.382 \text{ m s}^{-1}$ ,  $0.884 \text{ m s}^{-1}$  larger than that of 1-DOF GPEH. This demonstrates that the cut-in wind speed can be largely

reduced by a well-designed 2-DOF GPEH (such as 2-DOF GPEH-2). Notably, both 2-DOF GPEH configurations reach the maximum  $U_{cr}$  when  $R = 381 \text{ k}\Omega$ . The potential reason is that the circuit induced damping and stiffness of these two configurations are the same when given the same resistance according to equation (7). Thus, as the circuit induced damping reaches the peak, the maximum  $U_{cr}$  of 2-DOF GPEH is obtained for both configurations. In summary, compared to the conventional 1-DOF GPEH and 1-DOF GPEH-2, the 2-DOF GPEH-2 can efficiently reduce  $U_{cr}$ .

#### 4.2. Power output and efficiency

As an energy harvester, generating more power and improving the efficiency are two main targets that we pursue, hence, it is necessary to compare the power output and efficiency of conventional 1-DOF GPEH and that of the proposed 2-DOF GPEHs. For a fair comparison, all these energy harvesters have only one bluff body and all the bluff bodies are set to be same. The responses of these GPEHs are analytically calculated from equations (8), (10) and (12), and also numerically simulated by using the Runge–Kutta method. Three different resistances  $R = 10 \text{ k}\Omega$ ,  $400 \text{ k}\Omega$ ,  $1000 \text{ k}\Omega$  are considered in the comparison to represent small resistance (close to short circuit), medium resistance and large resistance (close to open circuit) respectively. Figure 3 shows the voltage responses of three configurations. First, it is noted that the analytical solutions obtained from the harmonic balance method can precisely predict the dynamic responses of both 1-DOF and 2-DOF GPEHs. Second, it is observed that for three different resistances,  $U_{cr}$  of 2-DOF GPEH-2 is the lowest while that of 2-DOF GPEH-1 is the highest, which is consistent with the prediction from the previous section. In terms of output voltage, the 2-DOF GPEH-2 has the largest output in the low-speed wind condition. For example, in figure 3(b) ( $R = 400 \text{ k}\Omega$ ), when  $U = 4 \text{ m s}^{-1}$ , the output voltages of 1-DOF GPEH, 2-DOF GPEH-1 and 2-DOF GPEH-2 are  $15.318 \text{ V}$ ,  $10.135 \text{ V}$  and  $16.787 \text{ V}$ , respectively. When  $U = 6 \text{ m s}^{-1}$ , the output voltage of these three energy harvesters are  $28.482 \text{ V}$ ,  $31.662 \text{ V}$  and  $27.3179 \text{ V}$ , respectively. Meanwhile, it is noted that in the high-speed wind condition, the conventional GPEH has a larger output when it is close to short circuit while the first configuration of 2-DOF GPEH has the largest output when it is close to the medium resistance or open circuit. Thus, the second configuration of 2-DOF GPEH is always preferable for low-speed wind energy harvesting regardless of resistance, while the first configuration of 2-DOF GPEH has the potential to increase the outputs of high-speed wind energy harvesting when the resistance is large.

Since the resistance in AC interface can largely affect the output power of energy harvesters, comparing the output voltages of the three configurations is not enough to illustrate the outperformance of 2-DOF GPEH. Hence, it is important to evaluate the performances of the three energy harvesters in terms of power output with varying resistance. Figure 4 shows the output powers of three configurations for three different wind speeds. Since the cut-in wind speed of these three configurations are largely different, the wind speeds ( $U$ )

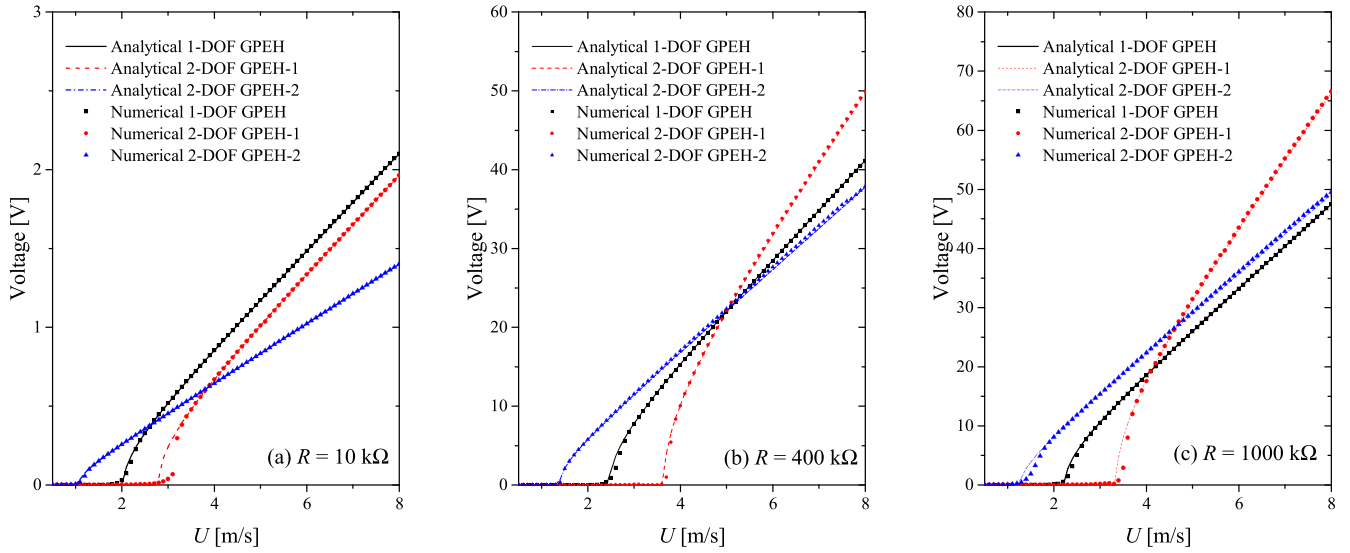


**Figure 3.** Analytical and numerical responses of 1-DOF and 2-DOF GPEHs: (a)  $R = 10 \text{ k}\Omega$ ; (b)  $R = 400 \text{ k}\Omega$ ; (c)  $R = 1000 \text{ k}\Omega$ .

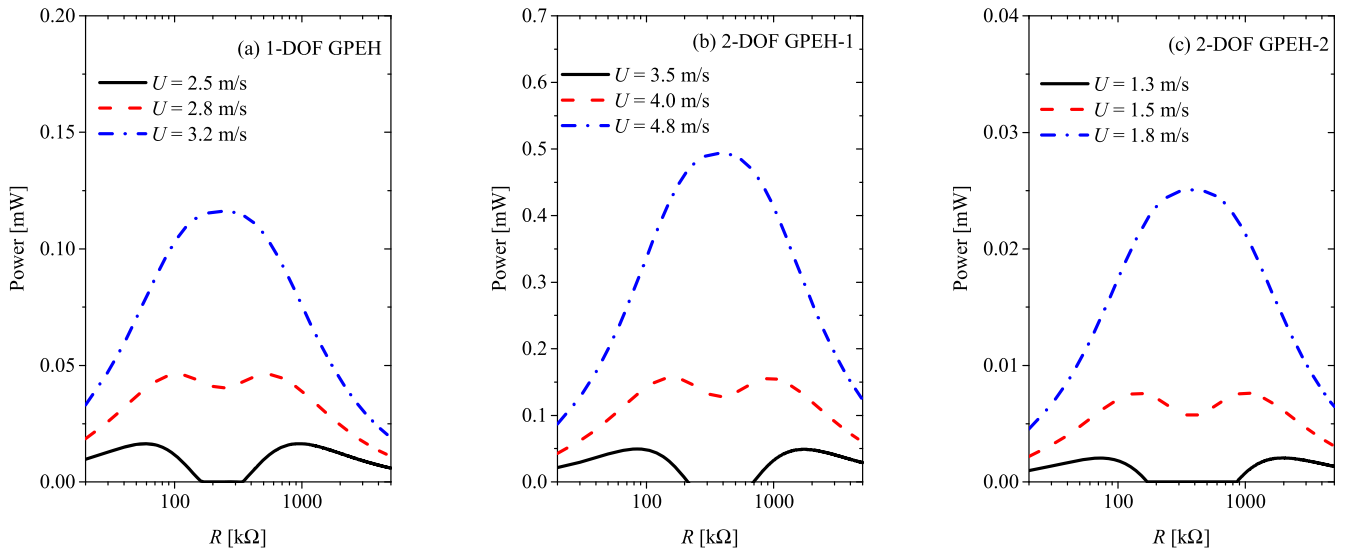


**Figure 4.** Output power of 1-DOF and 2-DOF GPEHs for varying resistances.

are carefully chosen so that the relations between resistance and generated power of these three configurations can be clearly depicted. It is found that the effects of resistance on these energy harvesters are similar. For example, for the small wind speed (close to the cut-in wind speed), two power peaks near the short circuit and open circuit respectively, are clearly obtained while no power is harvested for the medium resistance. The main reason is that the medium resistance can generate a large equivalent damping which increases the threshold of galloping and thus no electricity is produced. By increasing the wind speed, the galloping phenomenon can be attained for all resistances. In this case, two power peaks and one power valley are observed. With the further increase of wind speed, only one power peak is attained by these harvesters.

To fairly compare the output power of the three harvesters, their power peaks of their own optimal resistances

are furtherly shown in figure 5(a). It is noted that, for the low-speed wind ( $U < 4.3 \text{ m s}^{-1}$ ), the 2-DOF GPEH-2 has the highest power peaks; for the medium-speed wind ( $4.3 \text{ m s}^{-1} \leq U < 5.3 \text{ m s}^{-1}$ ), the conventional 1-DOF GPEH is the most efficient energy harvester; for the high-speed wind ( $U \geq 5.3 \text{ m s}^{-1}$ ), the 2-DOF GPEH-1 generates the largest power peaks. Hence, to increase the energy harvesting capability of low-speed wind energy, which widely exists in our daily life, the 2-DOF GPEH-2 is the most preferable design among the three configurations.

In addition to cut-in wind speed and output power, the swept area depending on the configuration are considered subsequently since it dictates how much flow energy is available to the device. The swept area can be calculated by

$$S_{\text{swept}} = L(D + 2Z), \quad (15)$$

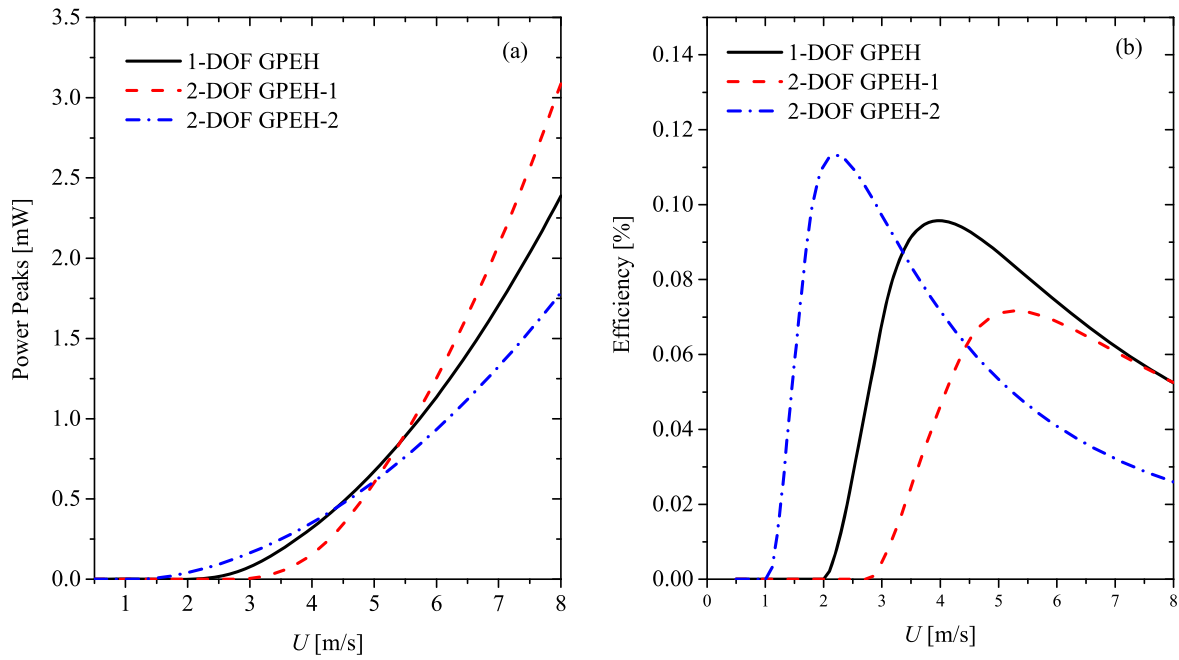


**Figure 5.** (a) Power peaks and (b) energy harvesting efficiencies of 1-DOF and 2-DOF GPEHs.

where  $Z$  is the displacement amplitude of an energy harvester. The wind power is defined as the kinetic energy flux of wind passing through the swept area and it is defined as

$$P_w = \frac{1}{2} \rho L (D + 2Z) U^3. \quad (16)$$

Hence, the efficiency of energy harvesting can be obtained

$$\lambda_e = \frac{P_e}{P_w} \times 100\%, \quad (17)$$

where  $P_e$  is the electrical power generated by an energy harvester, which is defined by equation (A.22).

Figure 5(a) has depicted the power peaks of their own optimal resistances of these three energy harvesters. Then, the corresponding efficiencies of three configurations can be obtained from equations (16) and (17), which is depicted in figure 5(b). It is revealed that the 2-DOF GPEH-2 has the highest peak efficiency, which is about 0.113%, while the peak efficiency of conventional 1-DOF GPEH and 2-DOF GPEH-1 are 0.0957% and 0.0713% respectively. In summary, a well-designed 2-DOF GPEH is beneficial to the decrease of the cut-in wind speed of conventional 1-DOF GPEH and the improvement of power generating efficiency of small wind energy harvesting.

## 5. Parametric study

In this section, to ascertain how to tune the 2-DOF GPEH-2 properly for achieving superior performance, the influences of system parameters including stiffness ( $k_1$  and  $k_2$ ), damping ( $c_1$  and  $c_2$ ), mass ( $m_1$  and  $m_2$ ) and resistance etc, on the cut-in wind speed and output power are investigated. The other parameters used in the analysis are kept the same as those listed in table 1. The responses of 2-DOF GPEH-2 are

predicted by using the harmonic balance method. Since the first configuration of 2-DOF GPEH fails to reduce the cut-in wind speed and one of our key objectives is to decrease the threshold of galloping. Hence the following parametric study will only focus on the 2-DOF GPEH-2.

### 5.1. Effects on cut-in wind speed

**5.1.1. Effects of stiffnesses.** Figure 6(a) presents the change of the cut-in wind speed ( $U_{cr}$ ) in response to the change of the stiffness  $k_1$  for different shunt resistances. It is noted that with the increase of  $k_1$ , the cut-in wind speed  $U_{cr}$  increases first with a fast rate, then slowly to a saturation value. In addition, the variation of the resistance does not change the effect of  $k_1$  on  $U_{cr}$ . Moreover, for a given  $k_1$ , when the shunt circuit is close to the open circuit (e.g. 1000 k $\Omega$ ) or short circuit condition (e.g. 10 k $\Omega$ ),  $U_{cr}$  becomes relatively small. While for a medium resistance (e.g. 500 k $\Omega$ ),  $U_{cr}$  is quite large. This phenomenon can be easily understood by recalling the effect of the shunt resistance on the electrical induced damping, which has already been discussed in the previous section.

Figure 6(b) shows the relationship between the stiffness  $k_2$  and the cut-in wind speed ( $U_{cr}$ ). It is found that when the resistance is different, the effect of  $k_2$  on  $U_{cr}$  is different. For a small resistance (e.g. 10 k $\Omega$ ), the cut-in wind speed increases monotonously with the increase of  $k_2$ . Under this situation,  $k_2$  is suggested to be tuned small for decreasing the threshold of galloping. However, when the resistance becomes larger (e.g. 1000 k $\Omega$ ), with the increase of  $k_2$ ,  $U_{cr}$  first increases quickly then decreases slowly. In addition, it is observed that when  $k_2$  further increases to approximately more than 200 N m $^{-1}$ , the effect of  $R$  becomes very weak and ignorable. Besides that, when  $k_2$  is close to zero, the resistance  $R$  plays a predominant role in the determination of the threshold of galloping. The potential reason is that, when  $k_2$  is small, the circuit induced

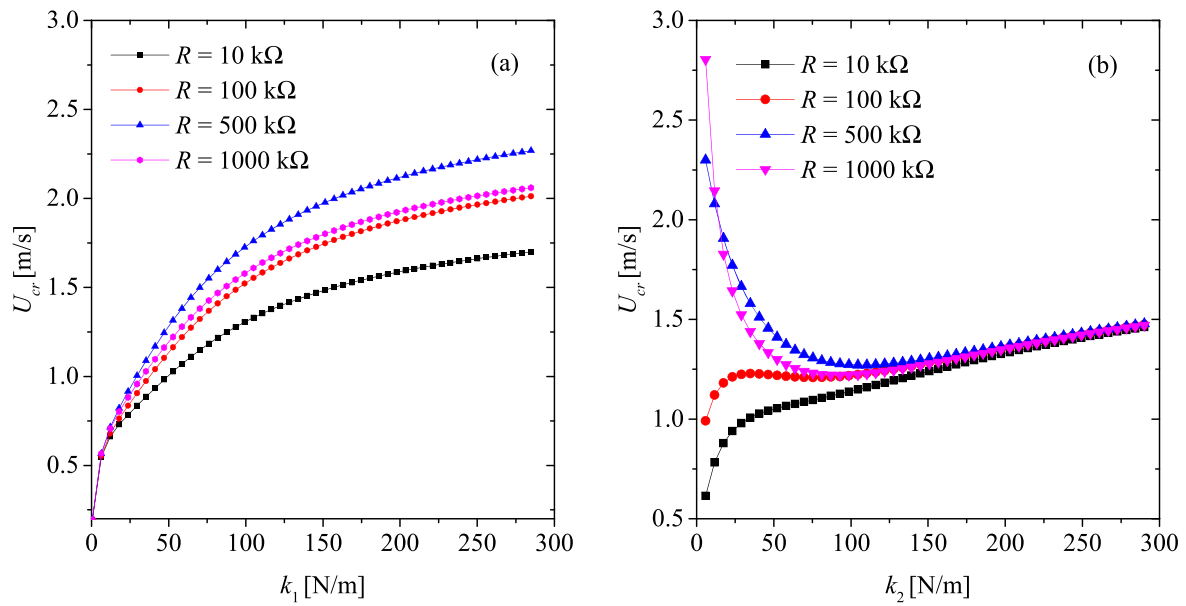


Figure 6. Effects of  $k_1$  and  $k_2$  on the cut-in wind speed ( $U_{cr}$ ) of 2-DOF GPEH-2: (a)  $k_1$ ; (b)  $k_2$ .

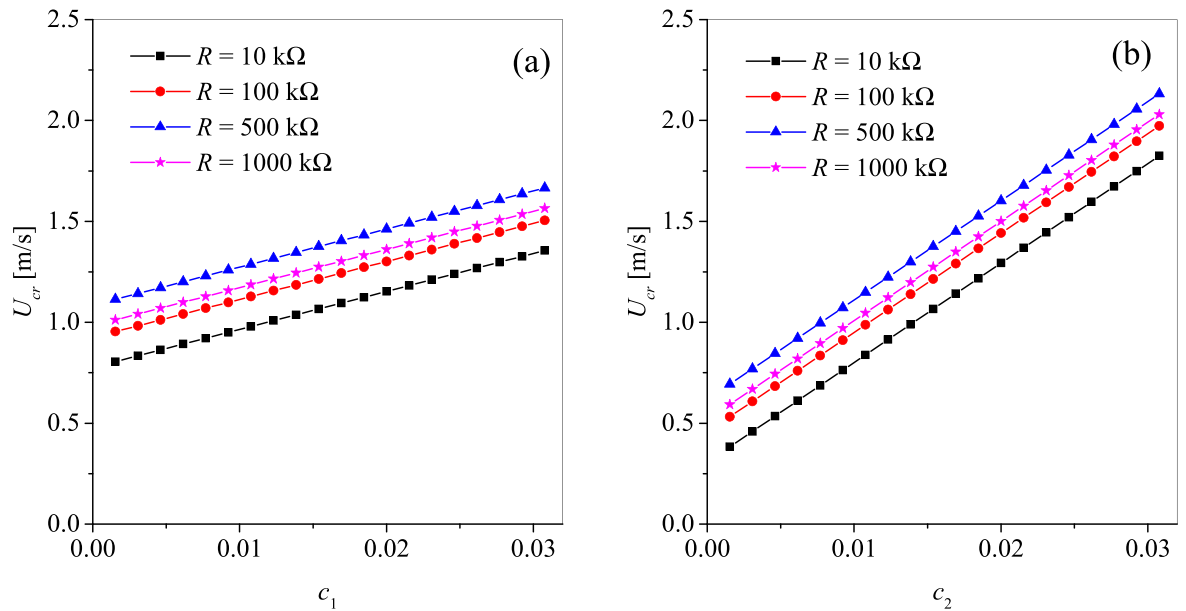


Figure 7. Effects of  $c_1$  and  $c_2$  on the cut-in wind speed ( $U_{cr}$ ) of 2-DOF GPEH-2: (a)  $c_1$ ; (b)  $c_2$ .

stiffness ( $k_e$ ) as shown in equation (7) has a significant contribution to the total effective stiffness of the whole system, which results in an evident influence on the circuit induced damping. As a result, the cut-in speed is closely related to the resistance. However, when  $k_2$  is very large, the circuit induced stiffness has only a minor effect on the total effective stiffness of the whole system and the circuit-induced damping. Hence, the thresholds  $U_{cr}$  for large resistances are almost the same.

In summary, to reduce the cut-in wind speed, a small  $k_1$  is always preferred while the selection of  $k_2$  depends on the resistance. For a small resistance, a small  $k_2$  is a better option to decrease  $U_{cr}$ . While for a large resistance, there exists an optimal  $k_2$  for achieving the lowest  $U_{cr}$ .

**5.1.2. Effects of mechanical damping.** Mechanical damping is another critical factor that largely affects the threshold of galloping, therefore, it is important to investigate the effects of damping on  $U_{cr}$ . The mechanical damping  $c_1$  and  $c_2$  are considered and the corresponding results are depicted in figure 7. It is noted that the cut-in wind speed  $U_{cr}$  increases with the increase of both  $c_1$  and  $c_2$  and this phenomenon holds for any resistance. As a result, a smaller damping always leads to a lower  $U_{cr}$ . Besides that, based on the comparison of figures 7(a) and (b), it is observed that  $U_{cr}$  is more sensitive to  $c_2$  than  $c_1$ . Therefore, decreasing  $c_2$  is a more efficient way to reduce  $U_{cr}$ .

**5.1.3. Effects of masses.** Figure 8 shows the effects of the masses  $m_1$  and  $m_2$  on the cut-in wind speed. Through the

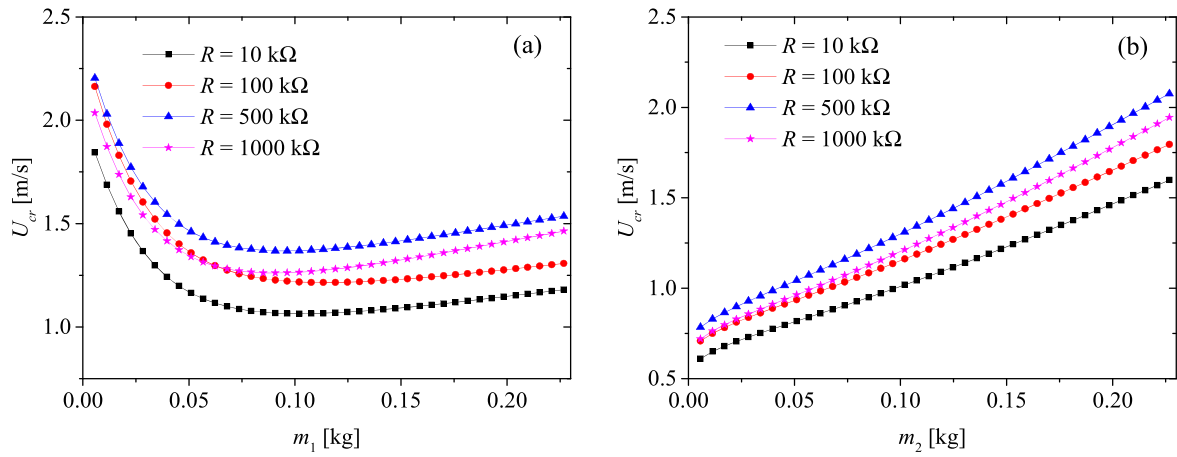


Figure 8. Effect of  $m_1$  and  $m_2$  on the cut-in wind speed ( $U_{cr}$ ) of 2-DOF GPEH-2: (a) effect of  $m_1$ ; (b) effect of  $m_2$ .

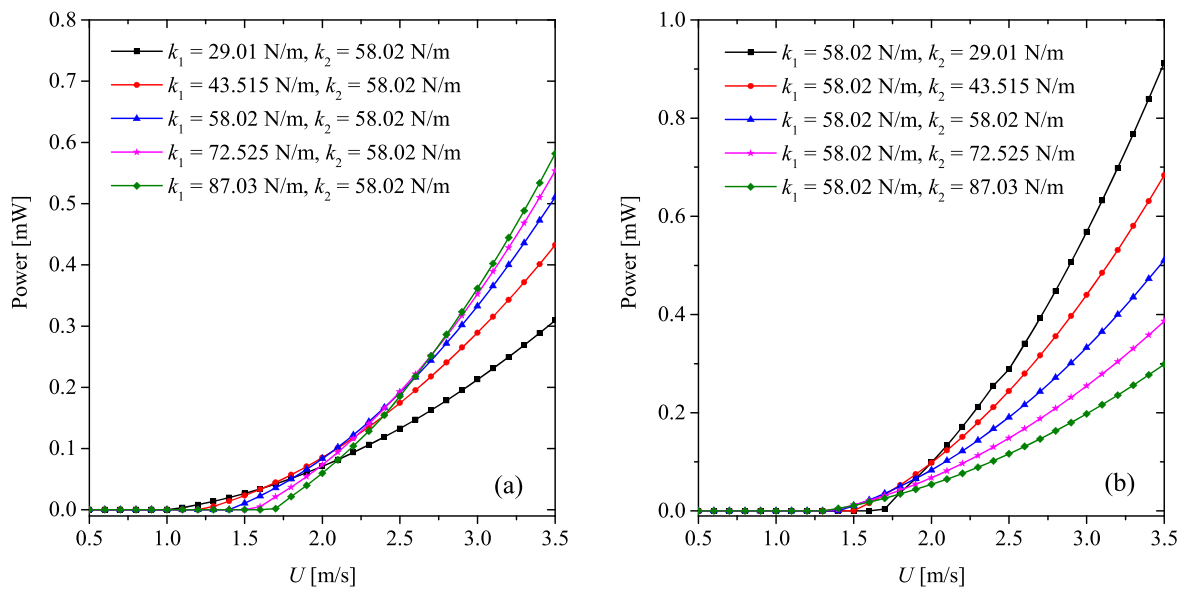


Figure 9. Power output of 2-DOF GPEH-2 for various  $k_1$  and  $k_2$ : (a)  $k_1$ ,  $R = 400$  k $\Omega$ ; (b)  $k_2$ ,  $R = 400$  k $\Omega$ .

comparison between figures 8(a) and (b), it is noted that the effects of  $m_1$  and  $m_2$  are different. With the increase of  $m_1$ , the cut-in wind speed first decreases then increases. Hence, there is an optimal  $m_1$  where the lowest  $U_{cr}$  can be obtained. Different from  $m_1$ ,  $U_{cr}$  monotonously increases with the increase of  $m_2$  (figure 8(b)). This trend is consistent for any resistance that varies from short circuit condition to the open circuit condition. As a result, in order to obtain a low  $U_{cr}$ ,  $m_2$  needs to always be small while  $m_1$  should be optimised for different resistances.

In summary, based on the parametric study results, several guidelines to reduce the cut-in wind speed are concluded as follows: firstly, the stiffnesses should be carefully tuned based on its relation with the resistance  $R$ ; secondly, the system damping is suggested to be reduced as much as possible; finally, a smaller  $m_2$  and an optimal  $m_1$  are recommended.

## 5.2. Effects on power output

**5.2.1. Effects of stiffnesses.** Figures 9(a) and (b) show the power output of 2-DOF GPEH-2 for various  $k_1$  and  $k_2$ ,

respectively. From figure 9(a), it can be seen that the increase of the stiffness  $k_1$  leads to increase of the cut-in wind speed, which is consistent with the conclusion obtained in section 5.1.1. Meanwhile, the output power is increased by decreasing  $k_1$  in the low-speed wind condition. However, in the relatively high-speed wind condition, such as  $U = 3.0$  m s $^{-1}$ , the generated power increases with the increase of  $k_1$ . Figure 10(a) presents the different relations of the power output and the stiffness  $k_1$  for different wind speeds. It is revealed that for the low-speed wind, such as  $U = 1.5$  m s $^{-1}$ , the power output increases with the increase of  $k_1$  before reaching the optimal  $k_1$  where the maximum power output is obtained. Beyond the optimal  $k_1$ , the further increase of  $k_1$  results in a decrease of power. The extreme case is that no power output is generated for a large  $k_1$ . However, for the high-speed wind, such as  $U = 5.0$  m s $^{-1}$ , the power output increases rapidly with the increase of  $k_1$  at the beginning. As  $k_1$  becomes quite large, the power output will reach the saturation. As can be seen that, although the increase of  $k_1$  will result in the increase of the cut-in wind speed

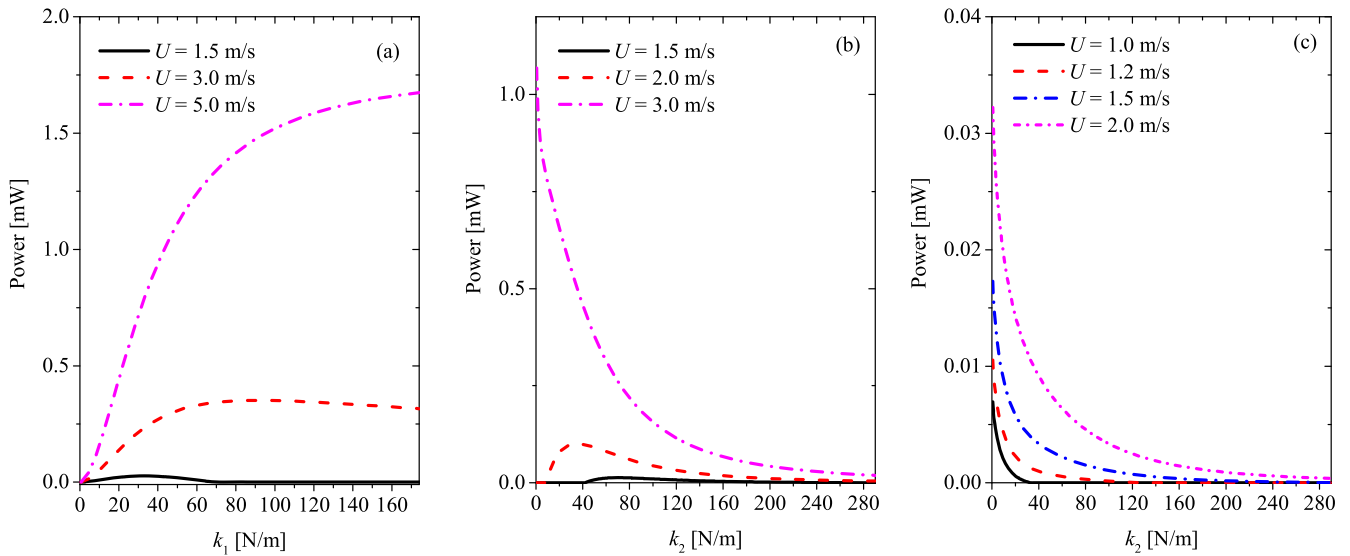


**Figure 10.** Effect of  $k_1$  and  $k_2$  on power output of 2-DOF GPEH-2: (a)  $k_1$ ,  $R = 400 \text{ k}\Omega$ ; (b)  $k_2$ ,  $R = 400 \text{ k}\Omega$ ; (c)  $k_2$ ,  $R = 10 \text{ k}\Omega$ .

(figure 6(a)), the power output for the high-speed wind energy is also improved dramatically. In conclusion, for the low-speed wind energy harvesting, an optimal  $k_1$  can be obtained to enhance the performance of 2-DOF GPEH under the premise of ensuring the occurrence of the galloping phenomenon. While for the high-speed wind energy harvesting when there is no concern about the cut-in wind speed i.e. the occurrence of the galloping phenomenon, a large  $k_1$  is preferable in terms of output voltage.

Figure 9(b) shows the effect of  $k_2$  on the power output of 2-DOF GPEH when  $R = 400 \text{ k}\Omega$ . It is noted that, on one hand, for the low-speed wind, the increase of  $k_2$  can reduce the cut-in wind speed when  $R = 400 \text{ k}\Omega$ ; on the other hand, for the high-speed wind condition, the increase of  $k_2$  leads to a decrease of power output. Since it is demonstrated as shown in figure 6(b) that the effect of  $k_2$  on the cut-in wind speed varies for different resistances, thus the resistance should also be considered when we analyse the relation between the power output and  $k_2$ . Figure 10(b) shows the power output by varying  $k_2$  when  $R = 400 \text{ k}\Omega$ . It is found that for the low speed wind, such as  $U = 1.5 \text{ m s}^{-1}$ , only when  $k_2 \in [42.93 \text{ N m}^{-1}, 290.1 \text{ N m}^{-1}]$  the system can generate electricity. If  $k_2$  is out of this range, no electrical energy can be produced. As the wind-speed increases to the medium level, such as  $U = 2 \text{ m s}^{-1}$ , this range can be extended and there exists an optimal  $k_2$  for achieving the maximum power output. For the wind speed becomes further larger, such as  $U = 3 \text{ m s}^{-1}$ , the increase of  $k_2$  lead to a decrease of power output instead. Moreover, for a small resistance (e.g.  $10 \text{ k}\Omega$ ) as shown in figure 10(c), the increase of  $k_2$  always results in the decrease of power output regardless of the wind speed.

**5.2.2. Effects of mechanical damping.** Figure 11 shows the effects of damping  $c_1$  and  $c_2$  on the power outputs of 2-DOF GPEH-2. The increase of the two damping coefficients results in the increase of the cut-in wind speed and the reduction of the power output, which is harmful for energy harvesting.

From the comparison of  $c_1$  and  $c_2$ , it is noted that  $c_2$  plays a more significant role in affecting the power output. Therefore, to satisfy the requirements of low cut-in wind speed and high output voltage, the damping should be as small as possible.

**5.2.3. Effects of masses.** Finally, the effect of mass,  $m_1$  and  $m_2$ , are evaluated in figure 12. It is indicated in figure 12(a) that the increase of  $m_1$  has a significant influence on the cut-in wind speed and the generated power of low-speed wind condition. When the wind speed is relatively large, the variation of  $m_1$  rarely affects the power output. It is worth mentioning that, it is also able to observe from figure 12(a) that the cut-in wind speed decreases with the increase of  $m_1$  when  $m_1$  is relatively small, while when  $m_1$  becomes relatively large, the relationship between the cut-in wind speed and  $m_1$  becomes inverse. This is consistent with the conclusion revealed in figure 8(a) that has been discussed in section 5.1.3. For the effect of  $m_2$  depicted in figure 12(b), it is found that an increase of  $m_2$  results in a decreased power output under the low-speed wind condition and an improved power under the high-speed wind condition. To further clearly show the effects of  $m_1$  and  $m_2$  on the power output for different wind speeds, the relations of power and mass are illustrated in figure 13. Under the low-speed wind condition, such as  $U = 1.5 \text{ m s}^{-1}$ , there is an optimal  $m_1$  that the maximum power is achieved and there is an upper-bound for  $m_2$  exceeds which, no electrical energy can be generated. However, the relation between the power and the mass in the high-speed wind condition differs a lot from that in the low-speed wind condition. First, the harvested power is not sensitive to the change of  $m_1$  and almost the same for different  $m_1$ . Second, an optimal  $m_2$  can be obtained to attain the peak power for the high-speed wind condition and this optimal  $m_2$  increases with the wind speed. These characteristics are useful to guide the optimisation of 2-DOF GPEH-2 for enhanced

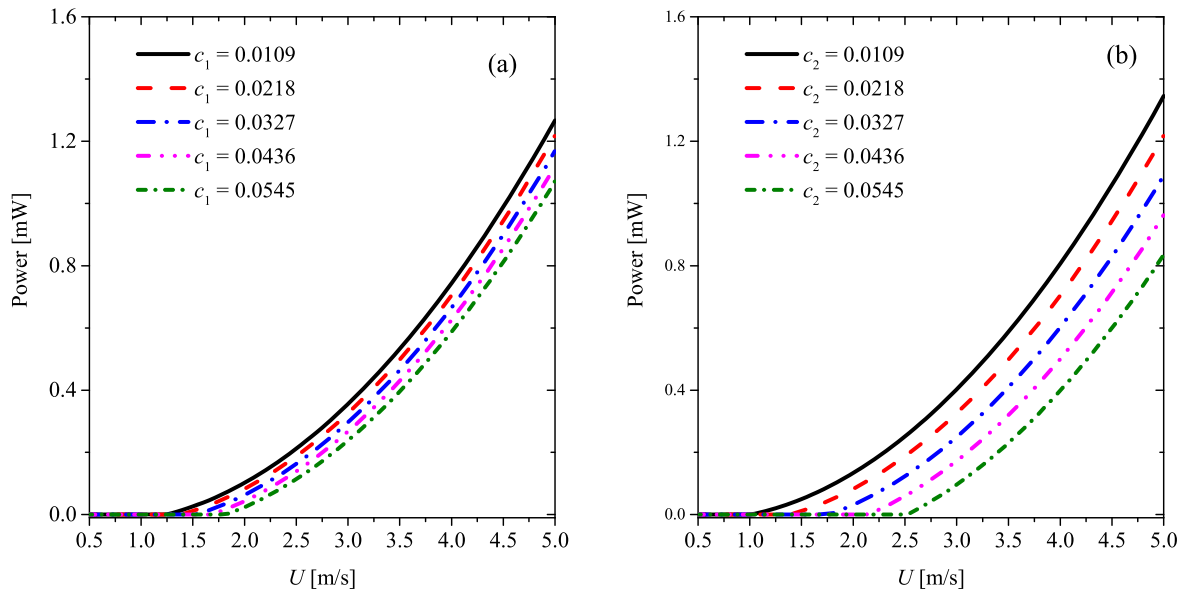


Figure 11. Effect of  $c_1$  and  $c_2$  on power output of 2-DOF GPEH-2: (a)  $c_1$ ,  $R = 400 \text{ k}\Omega$ ; (b)  $c_2$ ,  $R = 400 \text{ k}\Omega$ .

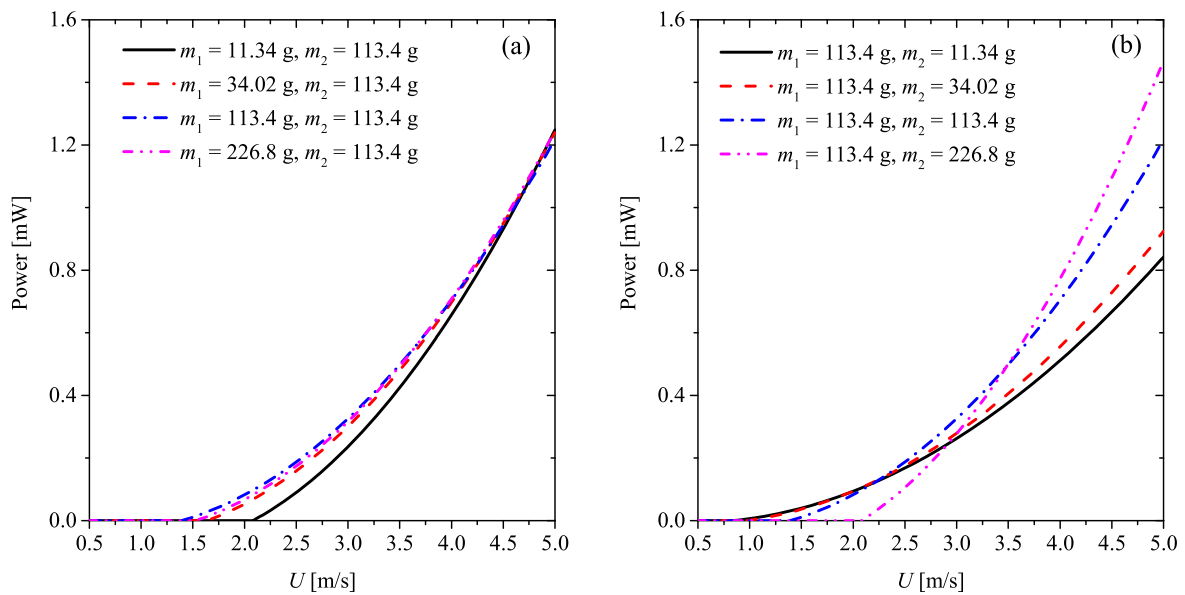


Figure 12. Effect of  $m_1$  and  $m_2$  on power output of 2-DOF GPEH-2: (a)  $m_1$ ,  $R = 400 \text{ k}\Omega$ ; (b)  $m_2$ ,  $R = 400 \text{ k}\Omega$ .

performance by adjusting  $m_1$  and  $m_2$  according to the wind conditions.

## 6. Conclusions

To reduce the cut-in wind speed and improve the output of the conventional 1-DOF galloping PEH, this paper develops two different configurations of 2-DOF GPEHs. The dynamic characteristics and energy harvesting performance of the two 2-DOF configurations and their potential advantages over the conventional 1-DOF GPEH are investigated. First, the harmonic balance method is utilised to derive the analytical solutions of both 1-DOF and 2-DOF GPEHs. Then, numerical simulations are conducted and the results agree very well with

the analytical predictions. From the comparison between the two 2-DOF configurations and the conventional 1-DOF counterpart, it is demonstrated that the second configuration of 2-DOF GPEH can easily reduce the cut-in wind speed and largely improve the output power of small wind energy harvesting, which is very promising to improve the efficiency of harvesting low-speed wind energy. Subsequently, a parametric study is conducted to ascertain the effects of the mechanical parameters on the cut-in wind speed and harvested power of 2-DOF GPEH-2. Some useful conclusions are drawn as follows:

- (1) The second configuration of 2-DOF GPEH (2-DOF GPEH-2) provides an efficient way to reduce the cut-in wind speed and enhance the power output, while the first

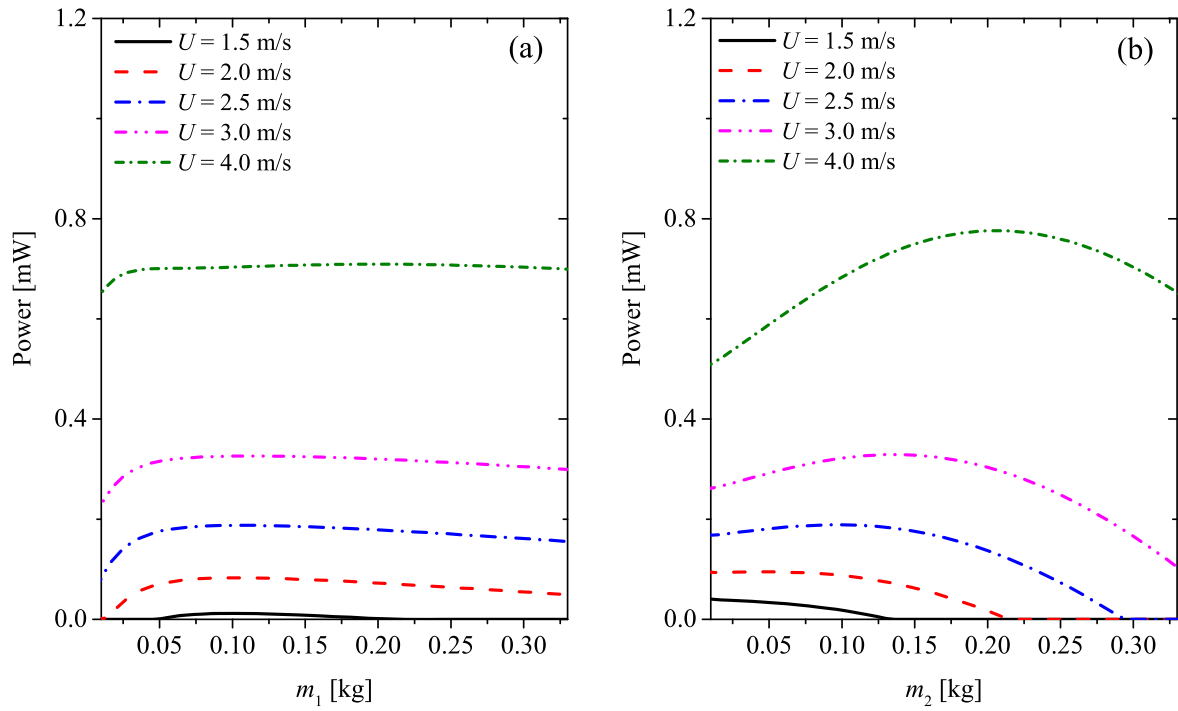


**Figure 13.** Effect of  $m_1$  and  $m_2$  on power output of 2-DOF GPEH-2 for different wind speeds: (a)  $m_1$ ,  $R = 400$  k $\Omega$ ; (b)  $m_2$ ,  $R = 400$  k $\Omega$ .

configuration (2-DOF GPEH-1) fails to maintain a lower cut-in wind speed but it still has the ability to improve the output under the high-speed wind condition.

- (2) To pursue a low cut-in wind speed, the parameters of 2-DOF GPEH-2 including the damping ( $c_1$  and  $c_2$ ), stiffness ( $k_1$ ) and mass ( $m_2$ ), are required to be small, while  $m_1$  can be optimised. The influence of  $k_2$  on the cut-in wind speed significantly depends on the resistance when  $k_2$  is not very large: when the resistance is small, a small  $k_2$  is always preferred; while for large resistances, an optimal  $k_2$  can be obtained;
- (3) Several ways to improve the output voltages of 2-DOF GPEH-2 are given as follows: the first method, which is not sensitive to the resistance, is to decrease the damping ( $c_1$  and  $c_2$ ); the second method, which is sensitive to the wind speed, is to optimise  $k_1$  and  $m_1$  in the low-speed wind condition while to increase  $k_1$  and optimise  $m_2$  in high-speed wind condition. The third method, which is sensitive to both the wind speed and the resistance, is to reduce  $k_2$  for the small resistance while for the large resistance,  $k_2$  should be optimised in low-speed wind condition and reduced in the high-speed condition.

## Acknowledgments

This study was supported by the New Staff Foundation of Nanjing University of Aeronautics and Astronautics (Grant No. 1001-YAH18051).

## Appendix

### Approximate analytical solutions of conventional 1-DOF GPEH

The governing equations of conventional 1-DOF GPEH are

$$\begin{cases} m_1 \ddot{x} + c_1 \dot{x} + k_1 x - \theta V = \frac{1}{2} \rho U L D \left[ s_1 \dot{x} - \frac{s_3}{U^2} (\dot{x})^3 \right] \\ C_p \dot{V} + \frac{V}{R} + \theta \dot{x} = 0 \end{cases} \quad (\text{A.1})$$

Assume the appropriate solutions have the following form

$$\begin{cases} x = a_1(t) \sin(\omega t) + b_1(t) \cos(\omega t) \\ V = a_3(t) \sin(\omega t) + b_3(t) \cos(\omega t) \\ \dot{x} = [\dot{a}_1(t) - \omega b_1(t)] \sin(\omega t) \\ \quad + [\omega a_1(t) + \dot{b}_1(t)] \cos(\omega t) \\ \dot{V} = [\dot{a}_3(t) - \omega b_3(t)] \sin(\omega t) \\ \quad + [\omega a_3(t) + \dot{b}_3(t)] \cos(\omega t) \\ \ddot{x} = [-\omega^2 a_1(t) - 2\omega \dot{b}_1(t)] \sin(\omega t) \\ \quad + [2\omega \dot{a}_1(t) - \omega^2 b_1(t)] \cos(\omega t) \end{cases} \quad (\text{A.2})$$

Substituting equation (A.2) into the first expression of equation (A.1), neglecting the higher harmonics and

balancing the terms of  $\sin(\omega t)$  and  $\cos(\omega t)$ , we obtain

$$\begin{aligned}
 & -m_1\omega^2 a_1(t) - c_1\omega b_1(t) + k_1 a_1 - \theta a_3 \\
 & + \frac{1}{2}\rho ULD \left( s_1 - \frac{3}{4} \frac{s_3}{U^2} \omega^2 (b_1^2(t) + a_1^2(t)) \right) \omega b_1(t) \\
 & = 2m_1\omega \dot{b}_1(t) - c_1 \dot{a}_1(t) \\
 & + \frac{1}{2}\rho ULD \left( s_1 - \frac{3}{4} \frac{s_3}{U^2} \omega^2 (b_1^2(t) + a_1^2(t)) \right) \dot{a}_1(t) \\
 & + \frac{1}{2}\rho ULD \left( -\frac{3}{4} \frac{s_3}{U^2} ((\dot{a}_1^2(t) + \dot{b}_1^2(t) \right. \\
 & \left. - 2\omega \dot{a}_1(t)b_1(t) + 2\omega a_1(t)\dot{b}_1(t))) (\dot{a}_1(t) - \omega b_1(t)) \right), \tag{A.3}
 \end{aligned}$$

$$\begin{aligned}
 & -m_1\omega^2 b_1(t) + c_1\omega a_1(t) + k_1 b_1 - \theta b_3 \\
 & - \frac{1}{2}\rho ULD \omega a_1(t) \left( s_1 - \frac{3}{4} \frac{s_3}{U^2} \omega^2 (b_1^2(t) + a_1^2(t)) \right) \\
 & = -2m_1\omega \dot{a}_1(t) - c_1 \dot{b}_1(t) \\
 & + \frac{1}{2}\rho ULD \dot{b}_1(t) \left( s_1 - \frac{3}{4} \frac{s_3}{U^2} \omega^2 (b_1^2(t) + a_1^2(t)) \right) \\
 & + \frac{1}{2}\rho ULD [\omega a_1(t) + \dot{b}_1(t)] \left( -\frac{3}{4} \frac{s_3}{U^2} (\dot{a}_1^2(t) + \dot{b}_1^2(t) \right. \\
 & \left. - 2\omega \dot{a}_1(t)b_1(t) + 2\omega a_1(t)\dot{b}_1(t)) \right). \tag{A.4}
 \end{aligned}$$

Applying the same procedure into the second expression of equation (A.1) yields

$$\frac{a_3(t)}{R} - \omega C_p b_3(t) - \omega \theta b_1(t) = -C_p \dot{a}_3(t) - \theta \dot{a}_1(t), \tag{A.5}$$

$$\frac{b_3(t)}{R} + \omega C_p a_3(t) + \omega \theta a_1(t) = -C_p \dot{b}_3(t) - \theta \dot{b}_1(t). \tag{A.6}$$

In the steady state, all time derivatives vanish so that equations (A.3)–(A.6) are simplified as

$$\begin{cases}
 -m_1\omega^2 a_1 - c_1\omega b_1 + k_1 a_1 - \theta a_3 \\
 + \frac{1}{2}\rho ULD \omega \left( s_1 - \frac{3}{4} \frac{s_3}{U^2} \omega^2 r^2 \right) b_1 = 0 \\
 -m_1\omega^2 b_1 + c_1\omega a_1 + k_1 b_1 - \theta b_3 \\
 - \frac{1}{2}\rho ULD \omega \left( s_1 - \frac{3}{4} \frac{s_3}{U^2} \omega^2 r^2 \right) a_1 = 0, \tag{A.7} \\
 \frac{a_3}{R} - \omega C_p b_3 - \omega \theta b_1 = 0 \\
 \frac{b_3}{R} + \omega C_p a_3 + \omega \theta a_1 = 0
 \end{cases}$$

where  $r^2 = a_1^2 + b_1^2$ .

By solving equation (A.7), we can obtain the approximate solutions of conventional 1-DOF GPEH, which is given as

$$\begin{cases}
 m_1\omega^2 - k_1 - \frac{C_p(\theta R\omega)^2}{(C_p R\omega)^2 + 1} = 0 \\
 c_1 + \frac{\theta^2 R}{(C_p R\omega)^2 + 1} - \frac{1}{2}\rho ULD \left( s_1 - \frac{3}{4} \frac{s_3}{U^2} \omega^2 r^2 \right) = 0
 \end{cases}. \tag{A.8}$$

*Approximate analytical solutions of 2-DOF GPEH-1*

The governing equations of 2-DOF GPEH-1 (refers to figure 1(b)) are

$$\begin{cases}
 m_1\ddot{x} + c_1(\dot{x} - \dot{y}) + k_1(x - y) = 0 \\
 m_2\ddot{y} + c_2\dot{y} + k_2y - \theta V \\
 = \frac{1}{2}\rho ULD \left[ s_1\dot{y} - \frac{s_3}{U^2} (\dot{y})^3 \right] + c_1(\dot{x} - \dot{y}) + k_1(x - y), \\
 C_p \dot{V} + \frac{V}{R} + \theta \dot{y} = 0
 \end{cases} \tag{A.9}$$

where  $m_2$ ,  $c_2$ , and  $k_2$ , are the effective mass, damping and stiffness of the auxiliary oscillator, respectively,  $y$  is the displacement of the auxiliary oscillator.

Assuming the appropriate solutions have the following form

$$\begin{cases}
 x = a_1(t) \sin(\omega t) + b_1(t) \cos(\omega t) \\
 y = a_2(t) \sin(\omega t) + b_2(t) \cos(\omega t) \\
 V = a_3(t) \sin(\omega t) + b_3(t) \cos(\omega t) \\
 \dot{x} = [\dot{a}_1(t) - \omega b_1(t)] \sin(\omega t) \\
 \quad + [\omega a_1(t) + \dot{b}_1(t)] \cos(\omega t) \\
 \dot{y} = [\dot{a}_2(t) - \omega b_2(t)] \sin(\omega t) \\
 \quad + [\omega a_2(t) + \dot{b}_2(t)] \cos(\omega t) \\
 \dot{V} = [\dot{a}_3(t) - \omega b_3(t)] \sin(\omega t) \\
 \quad + [\omega a_3(t) + \dot{b}_3(t)] \cos(\omega t) \\
 \ddot{x} = [-\omega^2 a_1(t) - 2\omega \dot{b}_1(t)] \sin(\omega t) \\
 \quad + [2\omega \dot{a}_1(t) - \omega^2 b_1(t)] \cos(\omega t) \\
 \ddot{y} = [-\omega^2 a_2(t) - 2\omega \dot{b}_2(t)] \sin(\omega t) \\
 \quad + [2\omega \dot{a}_2(t) - \omega^2 b_2(t)] \cos(\omega t)
 \end{cases}. \tag{A.10}$$

Substituting equation (A.10) into equation (A.9), neglecting the higher harmonics and balancing the terms of  $\sin(\omega t)$  and  $\cos(\omega t)$ , one obtains

$$\begin{aligned}
 & -m_1\omega^2 a_1(t) + c_1(-\omega b_1(t) + \omega b_2(t)) + k_1(a_1 - a_2) \\
 & = 2m_1\omega \dot{b}_1(t) - c_1(\dot{a}_1(t) - \dot{a}_2(t)), \tag{A.11a}
 \end{aligned}$$

$$\begin{aligned}
 & -m_1\omega^2 b_1(t) + c_1\omega(a_1(t) - a_2(t)) + k_1(b_1 - b_2) \\
 & = -2m_1\omega \dot{a}_1(t) - c_1\omega(\dot{b}_1(t) - \dot{b}_2(t)), \tag{A.11b}
 \end{aligned}$$

$$\begin{aligned}
 & -m_2\omega^2 a_2(t) - c_2\omega b_2(t) + c_1\omega(b_1(t) - b_2(t)) + k_2 a_2(t) \\
 & - \theta a_3(t) - k_1(a_1(t) - a_2(t)) \\
 & + \frac{1}{2}\rho ULD \left( s_1 - \frac{3}{4}\frac{s_3}{U^2}\omega^2(b_2^2(t) + a_2^2(t)) \right) \omega b_2(t) \\
 & = c_1(\dot{a}_1(t) - \dot{a}_2(t)) + 2m_2\omega \dot{b}_2(t) - c_2\dot{a}_2(t) \\
 & + \frac{1}{2}\rho ULD \left( s_1 - \frac{3}{4}\frac{s_3}{U^2}\omega^2(b_2^2(t) + a_2^2(t)) \right) \dot{a}_2(t) \\
 & + \frac{1}{2}\rho ULD \left( -\frac{3}{4}\frac{s_3}{U^2}(\dot{a}_2^2(t) + \dot{b}_2^2(t)) \right. \\
 & \left. - 2\omega\dot{a}_2(t)b_2(t) + 2\omega a_2(t)\dot{b}_2(t) \right) (\dot{a}_2(t) - \omega b_2(t)), \tag{A.11c}
 \end{aligned}$$

$$\begin{aligned}
 & -m_2\omega^2 b_2(t) + c_2\omega a_2(t) - c_1\omega(a_1(t) - a_2(t)) + k_2 b_2(t) \\
 & - \theta b_3(t) - k_1(b_1(t) - b_2(t)) \\
 & - \frac{1}{2}\rho ULD \omega a_2(t) \left( s_1 - \frac{3}{4}\frac{s_3}{U^2}\omega^2(b_2^2(t) + a_2^2(t)) \right) \\
 & = c_1(\dot{b}_1(t) - \dot{b}_2(t)) - 2m_2\omega \dot{a}_2(t) - c_2\dot{b}_2(t) \\
 & + \frac{1}{2}\rho ULD \dot{b}_2(t) \left( s_1 - \frac{3}{4}\frac{s_3}{U^2}\omega^2(b_2^2(t) + a_2^2(t)) \right) \\
 & + \frac{1}{2}\rho ULD [\omega a_2(t) + \dot{b}_2(t)] \left( -\frac{3}{4}\frac{s_3}{U^2}(\dot{a}_2^2(t) + \dot{b}_2^2(t)) \right. \\
 & \left. - 2\omega\dot{a}_2(t)b_2(t) + 2\omega a_2(t)\dot{b}_2(t) \right), \tag{A.11d}
 \end{aligned}$$

$$\frac{a_3(t)}{R} - \omega C_p b_3(t) - \omega \theta b_2(t) = -C_p \dot{a}_3(t) - \theta \dot{a}_2(t), \tag{A.11e}$$

$$\frac{b_3(t)}{R} + \omega C_p a_3(t) + \omega \theta a_2(t) = -C_p \dot{b}_3(t) - \theta \dot{b}_2(t). \tag{A.11f}$$

In the steady state, all time derivatives vanish so that equation (A.11) is simplified as

$$\begin{cases}
 -m_1\omega^2 a_1 + c_1\omega(-b_1 + b_2) + k_1(a_1 - a_2) = 0 \\
 -m_1\omega^2 b_1 + c_1\omega(a_1 - a_2) + k_1(b_1 - b_2) = 0 \\
 -m_2\omega^2 a_2 - c_2\omega b_2 + c_1\omega(b_1 - b_2) + k_2 a_2 - \theta a_3 \\
 \quad - k_1(a_1 - a_2) + \frac{1}{2}\rho ULD \omega b_2 \left( s_1 - \frac{3}{4}\frac{s_3}{U^2}\omega^2 \right. \\
 \quad \left. (b_2^2 + a_2^2) \right) = 0 \\
 -m_2\omega^2 b_2 + c_2\omega a_2 - c_1\omega(a_1 - a_2) + k_2 b_2 - \theta b_3. \tag{A.12} \\
 -k_1(b_1 - b_2) - \frac{1}{2}\rho ULD \omega a_2 \left( s_1 - \frac{3}{4}\frac{s_3}{U^2}\omega^2 \right. \\
 \quad \left. (b_2^2 + a_2^2) \right) = 0 \\
 \frac{a_3}{R} - \omega C_p b_3 - \omega \theta b_2 = 0 \\
 \frac{b_3}{R} + \omega C_p a_3 + \omega \theta a_2 = 0
 \end{cases}$$

Since the fifth and sixth expressions in equation (A.12) are linear, the electrical coefficients  $a_3$  and  $b_3$  can be solved as

$$\begin{cases}
 a_3 = \frac{-\theta C_p a_2 (R\omega)^2 + \theta R \omega b_2}{(C_p R \omega)^2 + 1} \\
 b_3 = \frac{-\theta C_p b_2 (R\omega)^2 - \theta R \omega a_2}{(C_p R \omega)^2 + 1}
 \end{cases} \tag{A.13}$$

Substituting the electrical stiffness and damping (equation (7)) into equation (A.13) gives

$$\begin{cases}
 a_3 = \frac{1}{\theta}(-k_{AC} a_2 + c_{AC} \omega b_2) \\
 b_3 = \frac{1}{\theta}(-k_{AC} b_2 - c_{AC} \omega a_2)
 \end{cases} \tag{A.14}$$

Substituting the steady-state solutions for  $a_3$  and  $b_3$  into the first and second expressions in equation (A.12) yields

$$\begin{cases}
 a_1 = \frac{(c_1\omega)^2 + (k_1 - m_1\omega^2)k_1}{(k_1 - m_1\omega^2)^2 + (c_1\omega)^2} a_2 \\
 \quad + \frac{m_1\omega^2 c_1\omega}{(k_1 - m_1\omega^2)^2 + (c_1\omega)^2} b_2 \\
 b_1 = -\frac{m_1 c_1 \omega^3}{(k_1 - m_1\omega^2)^2 + (c_1\omega)^2} a_2 \\
 \quad + \frac{(c_1\omega)^2 + (k_1 - m_1\omega^2)k_1}{(k_1 - m_1\omega^2)^2 + (c_1\omega)^2} b_2
 \end{cases} \tag{A.15}$$

Equation (A.15) can be rewritten as

$$\begin{cases}
 a_1 = p a_2 + q b_2 \\
 b_1 = -q a_2 + p b_2
 \end{cases} \tag{A.16}$$

where

$$\begin{aligned}
 p &= \frac{(c_1\omega)^2 + (k_1 - m_1\omega^2)k_1}{(k_1 - m_1\omega^2)^2 + (c_1\omega)^2}, \quad q \\
 &= \frac{m_1\omega^2 c_1\omega}{(k_1 - m_1\omega^2)^2 + (c_1\omega)^2}. \tag{A.17}
 \end{aligned}$$

Hence, the relation between  $r_x$  and  $r_y$  follows

$$r_y = \sqrt{p^2 + q^2} r_x, \tag{A.18}$$

where  $r_x = \sqrt{a_1^2 + b_1^2}$  and  $r_y = \sqrt{a_2^2 + b_2^2}$  are the displacement amplitudes of  $x$  and  $y$  respectively.

Subsequently, submitting equation (A.16) into the third and fourth expressions in equation (A.12) and solving the equations, one obtains

$$\begin{cases}
 [-m_2\omega^2 - c_1\omega q + \bar{k}_2 - k_1(p-1)]a_2 + [-\bar{c}_2\omega + c_1\omega(p-1) \\
 \quad - k_1 q + \frac{1}{2}\rho ULD \left( s_1 - \frac{3}{4}\frac{s_3}{U^2}\omega^2 r_y^2 \right) \omega] b_2 = 0 \\
 \left[ \bar{c}_2\omega - c_1\omega(p-1) + k_1 q - \frac{1}{2}\rho ULD \left( s_1 - \frac{3}{4}\frac{s_3}{U^2}\omega^2 r_y^2 \right) \omega \right] a_2 \\
 \quad + [-m_2\omega^2 - c_1\omega q + \bar{k}_2 - k_1(p-1)]b_2 = 0
 \end{cases} \tag{A.19}$$

where  $\bar{c}_2 = c_2 + c_e$ ,  $\bar{k}_2 = k_2 + k_e$ . Equation (A.19) can then

be further simplified as:

$$\begin{cases} -m_2\omega^2 - c_1\omega q + \bar{k}_2 - k_1(p-1) = 0 \\ -\bar{c}_2\omega + c_1\omega(p-1) - k_1q + \frac{1}{2}\rho ULD \\ \left(s_1 - \frac{3}{4}\frac{s_3}{U^2}\omega^2 r_y^2\right)\omega = 0 \end{cases} \quad (\text{A.20})$$

By solving equation (A.20), we can obtain the frequency of dynamic responses ( $\omega$ ) and the displacement amplitude  $r_y$ .

The output voltage  $V$  can be determined by equation (A.14) as

$$V = \sqrt{a_3^2 + b_3^2} = \frac{\theta R\omega}{\sqrt{(C_p R\omega)^2 + 1}} r_y. \quad (\text{A.21})$$

The output power is

$$P_e = \frac{V^2}{R} = \frac{R(\theta\omega)^2}{(C_p R\omega)^2 + 1} r_y^2. \quad (\text{A.22})$$

#### Approximate analytical solutions of 2-DOF GPEH-2

The governing equations of 2-DOF GPEH-2 (refers to figure 1(c)) are

$$\begin{cases} m_1\ddot{x} + c_1(\dot{x} - \dot{y}) + k_1(x - y) = \frac{1}{2}\rho ULD \left[ s_1\dot{x} - \frac{s_3}{U^2}(\dot{x})^3 \right] \\ m_2\ddot{y} + c_2\dot{y} + k_2y - \theta V = c_1(\dot{x} - \dot{y}) + k_1(x - y) \\ C_p\dot{V} + \frac{V}{R} + \theta y = 0 \end{cases} \quad (\text{A.23})$$

Similarly, the same procedure is employed to solve the approximate solutions of 2-DOF GPEH-2. Assuming the appropriate solutions have the same form as equation (A.10), substituting equation (A.10) into equation (A.23), neglecting the higher harmonics and balancing the terms of  $\sin(\omega t)$  and  $\cos(\omega t)$ , we obtain

$$\begin{aligned} & -m_1\omega^2 a_1(t) + c_1(-\omega b_1(t) + \omega b_2(t)) + k_1(a_1 - a_2) \\ & + \frac{1}{2}\rho ULD \left( s_1 - \frac{3}{4}\frac{s_3}{U^2}\omega^2(b_1^2(t) + a_1^2(t)) \right) \omega b_1(t) \\ & = m_1 2\omega \dot{b}_1(t) - c_1(\dot{a}_1(t) - \dot{a}_2(t)) \\ & + \frac{1}{2}\rho ULD \left( s_1 - \frac{3}{4}\frac{s_3}{U^2}\omega^2(b_1^2(t) + a_1^2(t)) \right) \dot{a}_1(t) \\ & + \frac{1}{2}\rho ULD \left( -\frac{3}{4}\frac{s_3}{U^2}(\dot{a}_1^2(t) + \dot{b}_1^2(t) - 2\omega \dot{a}_1(t)) \right) \\ & \times b_1(t) + 2\omega a_1(t) \dot{b}_1(t) \big) (\dot{a}_1(t) - \omega b_1(t)), \end{aligned} \quad (\text{A.24a})$$

$$\begin{aligned} & -m_1\omega^2 b_1(t) + c_1\omega(a_1(t) - a_2(t)) + k_1(b_1 - b_2) \\ & - \frac{1}{2}\rho ULD \omega a_1(t) \left( s_1 - \frac{3}{4}\frac{s_3}{U^2}\omega^2(b_1^2(t) + a_1^2(t)) \right) \\ & = -2m_1\omega \dot{a}_1(t) - c_1\omega(\dot{b}_1(t) - \dot{b}_2(t)) \\ & + \frac{1}{2}\rho ULD \dot{b}_1(t) \left( s_1 - \frac{3}{4}\frac{s_3}{U^2}\omega^2(b_1^2(t) + a_1^2(t)) \right) \\ & + \frac{1}{2}\rho ULD [\omega a_1(t) + \dot{b}_1(t)] \left( -\frac{3}{4}\frac{s_3}{U^2}(\dot{a}_1^2(t) + \dot{b}_1^2(t)) \right. \\ & \left. - 2\omega \dot{a}_1(t) b_1(t) + 2\omega a_1(t) \dot{b}_1(t) \right), \end{aligned} \quad (\text{A.24b})$$

$$\begin{aligned} & -m_2\omega^2 a_2(t) - c_2\omega b_2(t) + c_1\omega(b_1(t) - b_2(t)) + k_2 a_2 \\ & - \theta a_3 - k_1(a_1 - a_2) \\ & = c_1(\dot{a}_1(t) - \dot{a}_2(t)) + 2m_2\omega \dot{b}_2(t) - c_2 \dot{a}_2(t), \end{aligned} \quad (\text{A.24c})$$

$$\begin{aligned} & -m_2\omega^2 b_2(t) + c_2\omega a_2(t) - c_1\omega(a_1(t) - a_2(t)) + k_2 b_2 \\ & - \theta b_3 - k_1(b_1 - b_2) \\ & = c_1(\dot{b}_1(t) - \dot{b}_2(t)) - 2m_2\omega \dot{a}_2(t) - c_2 \dot{b}_2(t), \end{aligned} \quad (\text{A.24d})$$

$$\frac{a_3(t)}{R} - \omega C_p b_3(t) - \omega \theta b_2(t) = -C_p \dot{a}_3(t) - \theta \dot{a}_2(t), \quad (\text{A.24e})$$

$$\frac{b_3(t)}{R} + \omega C_p a_3(t) + \omega \theta a_2(t) = -C_p \dot{b}_3(t) - \theta \dot{b}_2(t). \quad (\text{A.24f})$$

Since all the time derivatives vanish in the steady state, that equation (A.24) is simplified as

$$\begin{cases} -m_1\omega^2 a_1 + c_1(-\omega b_1 + \omega b_2) + k_1(a_1 - a_2) \\ + \frac{1}{2}\rho ULD \left( s_1 - \frac{3}{4}\frac{s_3}{U^2}\omega^2(b_1^2 + a_1^2) \right) \omega b_1 = 0 \\ -m_1\omega^2 b_1 + c_1\omega(a_1 - a_2) + k_1(b_1 - b_2) \\ - \frac{1}{2}\rho ULD \omega a_1 \left( s_1 - \frac{3}{4}\frac{s_3}{U^2}\omega^2(b_1^2 + a_1^2) \right) = 0 \\ -m_2\omega^2 a_2 - c_2\omega b_2 + c_1\omega(b_1 - b_2) + k_2 a_2 - \theta a_3 \\ - k_1(a_1 - a_2) = 0 \\ -m_2\omega^2 b_2 + c_2\omega a_2 - c_1\omega(a_1 - a_2) + k_2 b_2 - \theta b_3 \\ - k_1(b_1 - b_2) = 0 \\ \frac{a_3}{R} - \omega C_p b_3 - \omega \theta b_2 = 0 \\ \frac{b_3}{R} + \omega C_p a_3 + \omega \theta a_2 = 0 \end{cases} \quad (\text{A.25})$$

Notably, since the fifth and sixth expressions of equation (A.25) are same with that of equation (A.12), equations (A.13) and (A.14) are still valid for 2-DOF GPEH-2. Thus, substituting equations (A.13) and (A.14) into the third and fourth expressions of equation (A.25) gives

$$\begin{cases} -m_2\omega^2 a_2 - \bar{c}_2\omega b_2 + c_1\omega(b_1 - b_2) + \bar{k}_2 a_2 - k_1 \\ \quad \times (a_1 - a_2) = 0 \\ -m_2\omega^2 b_2 + \bar{c}_2\omega a_2 - c_1\omega(a_1 - a_2) + \bar{k}_2 b_2 \\ \quad - k_1(b_1 - b_2) = 0 \end{cases} \quad (\text{A.26})$$

By rearranging equation (A.26), we obtain

$$\begin{cases} a_2 = \bar{p}a_1 - \bar{q}b_1 \\ b_2 = \bar{q}a_1 + \bar{p}b_1 \end{cases} \quad (\text{A.27})$$

where

$$\begin{aligned} \bar{p} &= \frac{k_1(-m_2\omega^2 + \bar{k}_2 + k_1) + c_1\omega(\bar{c}_2\omega + c_1\omega)}{(-m_2\omega^2 + \bar{k}_2 + k_1)^2 + (\bar{c}_2\omega + c_1\omega)^2}, \\ \bar{q} &= \frac{-k_1(\bar{c}_2\omega + c_1\omega) + c_1\omega(-m_2\omega^2 + \bar{k}_2 + k_1)}{(\bar{c}_2\omega + c_1\omega)^2 + (-m_2\omega^2 + \bar{k}_2 + k_1)^2}. \end{aligned} \quad (\text{A.28})$$

Hence, the amplitudes of the displacements are related by

$$r_y = \sqrt{\bar{p}^2 + \bar{q}^2} r_x. \quad (\text{A.29})$$

By submitting equation (A.28) into equation (A.29), we obtain

$$r_y = r_x \sqrt{\frac{k_1^2 + c_1^2\omega^2}{(-m_2\omega^2 + \bar{k}_2 + k_1)^2 + (\bar{c}_2\omega + c_1\omega)^2}}. \quad (\text{A.30})$$

Subsequently, by submitting equation (A.27) into the first and second expressions in equation (A.25) and solving the equations, we obtained

$$\begin{cases} [-m_1\omega^2 + c_1\omega\bar{q} + k_1(1 - \bar{p})]a_1 + \left[ k_1\bar{q} - c_1\omega(1 - \bar{p}) \right. \\ \quad \left. + \frac{1}{2}\rho ULD\omega \left( s_1 - \frac{3}{4}\frac{s_3}{U^2}\omega^2 r_x^2 \right) \right] b_1 = 0 \\ [-m_1\omega^2 + c_1\omega\bar{q} + k_1(1 - \bar{p})]b_1 - \left[ k_1\bar{q} - c_1\omega(1 - \bar{p}) \right. \\ \quad \left. + \frac{1}{2}\rho ULD\omega \left( s_1 - \frac{3}{4}\frac{s_3}{U^2}\omega^2 r_x^2 \right) \right] a_1 = 0 \end{cases} \quad (\text{A.31})$$

Since  $a_1$  and  $b_1$  are nonzeros, it implies that

$$\begin{cases} -m_1\omega^2 + c_1\omega\bar{q} + k_1(1 - \bar{p}) = 0 \\ k_1\bar{q} - c_1\omega(1 - \bar{p}) + \frac{1}{2}\rho ULD\omega \left( s_1 - \frac{3}{4}\frac{s_3}{U^2}\omega^2 r_x^2 \right) = 0 \end{cases} \quad (\text{A.32})$$

By solving equation (A.32), we can obtain the frequency of dynamic responses ( $\omega$ ) and the magnitudes of displacement responses  $r_x$  of 2-DOF GPEH-2. The output voltage  $V$  and power  $P_e$  of 2-DOF GPEH-2 can also be determined by equations (A.21) and (A.22).

## ORCID iDs

Chunbo Lan  <https://orcid.org/0000-0001-5959-0488>  
Lihua Tang  <https://orcid.org/0000-0001-5273-9294>

## References

- [1] Bernitsas M M, Raghavan K, Ben-Simon Y and Garcia E 2008 VIVACE (Vortex Induced Vibration Aquatic Clean Energy): a new concept in generation of clean and renewable energy from fluid flow *J. Offshore Mech. Arctic Eng.* **130** 041101
- [2] Kuang Y, Daniels A and Zhu M 2017 A sandwiched piezoelectric transducer with flex end-caps for energy harvesting in large force environments *J. Phys. D: Appl. Phys.* **50** 345501
- [3] Priya S and Inman D J 2009 *Energy Harvesting Technologies* (Berlin: Springer)
- [4] Marin A, Bressers S and Priya S 2011 Multiple cell configuration electromagnetic vibration energy harvester *J. Phys. D: Appl. Phys.* **44** 295501
- [5] Daqaq M F, Masana R, Erturk A and Quinn D D 2014 On the role of nonlinearities in vibratory energy harvesting: a critical review and discussion *Appl. Mech. Rev.* **66** 040801
- [6] Rostami A B and Armandei M 2017 Renewable energy harvesting by vortex-induced motions: review and benchmarking of technologies *Renew. Sustain. Energy Rev.* **70** 193–214
- [7] Abdelkefi A 2016 Aeroelastic energy harvesting: a review *Int. J. Eng. Sci.* **100** 112–35
- [8] Yang Z, Zhou S, Zu J and Inman D 2018 High-Performance piezoelectric energy harvesters and their applications *Joule* **2** 642–97
- [9] Liu W, Badel A, Formosa F, Zhu Q, Zhao C and Hu G 2018 A comprehensive analysis and modeling of the self-powered synchronous switching harvesting circuit with electronic breakers *IEEE Trans. Ind. Electron.* **65** 3899–909
- [10] Zhang M and Wang J 2016 Experimental study on piezoelectric energy harvesting from vortex-induced vibrations and wake-induced vibrations *J. Sensors* **2016** 2673292
- [11] Doare O and Michelin S 2011 Piezoelectric coupling in energy-harvesting fluttering flexible plates: linear stability analysis and conversion efficiency *J. Fluid Struct* **27** 1357–75
- [12] Shoele K and Mittal R 2016 Energy harvesting by flow-induced flutter in a simple model of an inverted piezoelectric flag *J. Fluid Mech.* **790** 582–606
- [13] Barrero-Gil A, Alonso G and Sanz-Andres A 2010 Energy harvesting from transverse galloping *J. Sound Vib.* **329** 2873–83
- [14] Abdelkefi A, Yan Z and Hajj M R 2013 Modeling and nonlinear analysis of piezoelectric energy harvesting from transverse galloping *Smart Mater. Struct.* **22** 025016
- [15] Ewere F, Wang G and Cain B 2014 Experimental investigation of galloping piezoelectric energy harvesters with square bluff bodies *Smart Mater. Struct.* **23** 104012
- [16] Yang Y, Zhao L and Tang L 2013 Comparative study of tip cross-sections for efficient galloping energy harvesting *Appl. Phys. Lett.* **102** 064105
- [17] Bibo A, Alhadidi A H and Daqaq M F 2015 Exploiting a nonlinear restoring force to improve the performance of flow energy harvesters *J. Appl. Phys.* **117** 045103
- [18] Bibo A and Daqaq M F 2015 An analytical framework for the design and comparative analysis of galloping energy harvesters under quasi-steady aerodynamics *Smart Mater. Struct.* **24** 094006

- [19] Akaydin H D, Elvin N and Andreopoulos Y 2010 Wake of a cylinder: a paradigm for energy harvesting with piezoelectric materials *Exp. Fluids* **49** 291–304
- [20] Jung H J and Lee S W 2011 The experimental validation of a new energy harvesting system based on the wake galloping phenomenon *Smart Mater. Struct.* **20** 055022
- [21] Alhadidi A H, Abderrahmane H and Daqaq M F 2016 Exploiting stiffness nonlinearities to improve flow energy capture from the wake of a bluff body *Physica D* **337** 30–42
- [22] Sirohi J and Mahadik R 2012 Harvesting wind energy using a galloping piezoelectric beam *J. Vib. Acoust.* **134** 011009
- [23] Sirohi J and Mahadik R 2011 Piezoelectric wind energy harvester for low-power sensors *J. Intell. Mater. Syst. Struct.* **22** 2215–28
- [24] Abdelkefi A, Hajj M R and Nayfeh A H 2012 Power harvesting from transverse galloping of square cylinder *Nonlinear Dyn.* **70** 1355–63
- [25] Zhao L Y, Tang L H and Yang Y W 2013 Comparison of modeling methods and parametric study for a piezoelectric wind energy harvester *Smart Mater. Struct.* **22** 125003
- [26] Abdelkefi A, Yan Z and Hajj M R 2013 Nonlinear dynamics of galloping-based piezoaeroelastic energy harvesters *Eur. Phys. J. Spec. Top.* **222** 1483–501
- [27] Parkinson G V and Brooks N P H 1961 On the aeroelastic instability of bluff cylinders *J. Appl. Mech.* **28** 252–8
- [28] Javed U and Abdelkefi A 2017 Impacts of the aerodynamic force representation on the stability and performance of a galloping-based energy harvester *J. Sound Vib.* **400** 213–26
- [29] Tang L H, Zhao L Y, Yang Y W and Lefeuvre E 2015 Equivalent circuit representation and analysis of galloping-based wind energy harvesting *IEEE/ASME Trans. Mechatronics* **20** 834–44
- [30] Tan T and Yan Z 2016 Analytical solution and optimal design for galloping-based piezoelectric energy harvesters *Appl. Phys. Lett.* **109** 253902
- [31] Zhao L Y and Yang Y W 2015 Analytical solutions for galloping-based piezoelectric energy harvesters with various interfacing circuits *Smart Mater. Struct.* **24** 075023
- [32] Bibo A, Abdelkefi A and Daqaq M F 2015 Modeling and characterization of a piezoelectric energy harvester under combined aerodynamic and base excitations *J. Vib. Acoust.* **137** 031017
- [33] Yan Z M and Abdelkefi A 2014 Nonlinear characterization of concurrent energy harvesting from galloping and base excitations *Nonlinear Dyn.* **77** 1171–89
- [34] Yan Z M, Abdelkefi A and Hajj M R 2014 Piezoelectric energy harvesting from hybrid vibrations *Smart Mater. Struct.* **23** 025026
- [35] Xu J and Tang J 2017 Modeling and analysis of piezoelectric cantilever-pendulum system for multi-directional energy harvesting *J. Intell. Mater. Syst. Struct.* **28** 323–38
- [36] Xiong L, Tang L, Liu K and Mace B R 2018 Broadband piezoelectric vibration energy harvesting using a nonlinear energy sink *J. Phys. D: Appl. Phys.* **51** 185502
- [37] Naseer R, Dai H L, Abdelkefi A and Wang L 2017 Piezomagnetoelastic energy harvesting from vortex-induced vibrations using monostable characteristics *Appl. Energy* **203** 142–53
- [38] Zhao L Y and Yang Y W 2018 An impact-based broadband aeroelastic energy harvester for concurrent wind and base vibration energy harvesting *Appl. Energy* **212** 233–43
- [39] Lan C, Tang L and Harn R L 2018 Comparative methods to assess harmonic response of nonlinear piezoelectric energy harvesters interfaced with AC and DC circuits *J. Sound Vib.* **421** 61–78
- [40] Zhao L, Tang L and Yang Y 2014 Enhanced piezoelectric galloping energy harvesting using 2 degree-of-freedom cut-out cantilever with magnetic interaction *Japan. J. Appl. Phys.* **53** 060302
- [41] Bibo A and Daqaq M 2014 On the optimal performance and universal design curves of galloping energy harvesters *Appl. Phys. Lett.* **104** 023901
- [42] Paidoussis M P, Price S J and Langre E D 2010 *Fluid-Structure Interactions: Cross-Flow-Induced Instabilities* (Cambridge: Cambridge University Press)
- [43] Parkinson G and Smith J 1964 The square prism as an aeroelastic non-linear oscillator *Q. J. Mech. Appl. Math.* **17** 225–39